

Theory of self-assembly of microtubules and motors

Igor S. Aranson¹ and Lev S. Tsimring²

¹Argonne National Laboratory, 9700 South Cass Avenue, Argonne, Illinois, 60439

²Institute for Nonlinear Science, University of California, San Diego, La Jolla, CA 92093-0402

(Dated: June 14, 2018)

We derive a model describing spatio-temporal organization of an array of microtubules interacting via molecular motors. Starting from a stochastic model of inelastic polar rods with a generic anisotropic interaction kernel we obtain a set of equations for the local rods concentration and orientation. At large enough mean density of rods and concentration of motors, the model describes an orientational instability. We demonstrate that the orientational instability leads to the formation of vortices and (for large density and/or kernel anisotropy) asters seen in recent experiments. We derive the specific form of the interaction kernel from the detailed analysis of microscopic interaction of two filaments mediated by a moving molecular motor, and extend our results to include variable motor density and motor attachment to the substrate.

PACS numbers: 87.16.-b, 05.65.+b, 47.55.+r

I. INTRODUCTION

One of the most important functions of molecular motors is to organize a network of long filaments (microtubules) during cell division to form cytoskeletons of daughter cells [1]. In order to better understand the details of this complex self-organization process, a number of *in vitro* experiments were performed [2, 3, 4, 5, 6, 7] to study interaction of molecular motors and microtubules in isolation from other biophysical processes simultaneously occurring *in vivo*. At large enough concentration of molecular motors and microtubules, the latter organize in *asters* and *vortices* depending on the type and concentration of molecular motors.

In the above experiments the elementary interaction processes were identified. After molecular motor binds to a microtubule at a random position, it marches along it in a fixed direction until it unbinds without appreciable displacement of microtubules (since the mass of a molecular motor is small in comparison with that of the microtubule). However, if a molecular motor binds to *two* microtubules (most molecular motors have at least two binding sites), it can change their mutual position and orientation significantly. In small-scale simulations [5], the interaction of rod-like filaments via motor binding has been studied, and patterns resembling experimental

ones were observed. In [8] a phenomenological model for the molecular motor density and the microtubule orientation has been proposed. The model included transport of molecular motors along microtubules and alignment of microtubules mediated by molecular motors. Simulations showed that vortices and asters indeed form in this model, however, only one large vortex formed in case of high density of motors. Ref. [9] generalized this model by including separate densities of free and bound molecular motors, as well as the density of microtubules. This model exhibited a transition from asters to vortices as the density of molecular motors is increased, in apparent disagreement with experimental evidence [7] that asters give way to vortices with *decreasing* the molecular motors concentration. Somewhat similar approach was employed more recently by Sankararaman et al. [10], again with the same apparent disagreement with the experiment as in Refs. [8, 9]. A phenomenological flux-force relation for active gels was introduced in [11]. While vortex and aster solutions were obtained in a certain limit, an analysis of that model is difficult because of the large number of unknown parameters and fields.

In Ref. [12] a set of equations for microtubules density and orientation was derived from conservation laws for microtubules probability distribution function. These conservation laws were based on the phenomenological expressions for the probability fluxes due to diffusion and motor-mediated interactions. The latter, however, assumed that tubules are only displaced and rotated infinitesimally in individual interactions, which may not be the case in experiments. The model does not produce onset of spontaneous orientation for any density of microtubules. The authors argue that asters and vortices may be created as a result of the “bundling instability” [13]. However, this model demonstrated the bundling instability at small densities of tubules, and oscillatory orientational instability at large densities contrary to observations in which the orientational ordering is observed at smaller densities and is not oscillatory. In subsequent publication [14], a derivation of the probability conser-

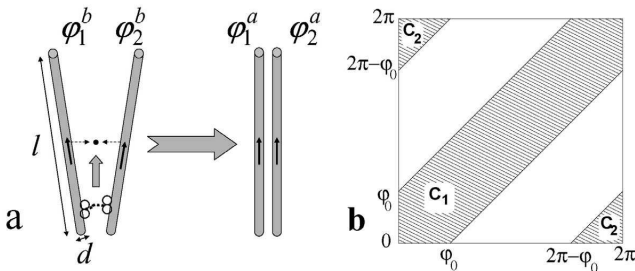


FIG. 1: a - sketch of motor-mediated two-rod interaction for $\gamma = 1/2$, b - integration regions $C_{1,2}$ for Eq.(2).

vation equations from microscopic mean-field model of forces between tubules and motors was presented, however the assumptions made in the course of derivation (i.e. infinitely stiff molecular motors) lead to a surprising conclusion that filaments do not change their orientation during interaction.

In this paper we present an alternative calculation of the microscopic motion of two filaments connected by a moving motor in a viscous fluid and show that filaments do change orientation as a result of the interaction. In our short publication [15] we derived a continuum model for the collective spatio-temporal dynamics of microtubules starting with a stochastic microscopic master equation for interacting inelastic polar rods, assuming that the density of molecular motors is homogeneous in space. Our model differed from the transport equations [12] in that it treated the interaction between two tubules as an instantaneous inelastic “collision” that can change the orientation of the filaments significantly. The model exhibits an onset of orientational order for large enough density of microtubules and molecular motors [16], formation of vortices and then asters with increase in the molecular motors concentration, in a qualitative agreement with experiment.

In this paper we present a more detailed derivation of our equations starting from a microscopic model of tubule-motor interaction. We derive the interaction kernel from microscopic rules and relate the kernel characteristics with the properties of the motors. We further extend our analysis: we lift the assumption of the homogeneous distribution of molecular motors and include an additional equation for the evolution of the molecular motor density. We also consider the situation when some molecular motors are attached to a substrate (usually, a glass plate). These modifications allow us to improve an agreement with experiment. We explain accumulation of molecular motors at the center of an aster by advection along microtubules and slow rotation of vortices by the interaction of microtubules with the attached motors, as it was observed in experiments.

The structure of the paper is as follows. In Sec. II we present derivation of the coarse-grained equation for orientation and density from the microscopic Maxwell model for interacting polar rods. In Sec. III we calculate the form of the interaction kernel from microscopic rules of interaction of two filaments. In Sec. IV the effects of spatial coupling are considered. First in Sec. IV A we reduce stochastic equations for the probability function to the set of equations for local orientation and density of microtubules. In Sec. IV B the stability analysis of the isolated vortex and aster solutions is performed and the phase diagram of various regimes is presented as the function of motor density and anisotropy of the interaction kernel. In Sec. V we include effects of motors attached to the substrate and explain rotation of the vortices and onset of large variations of the microtubules density. In Sec. VI we consider effects of variable motor density and derive the equation for the evolution of the motors. Tech-

nical details of derivations are presented in Appendices.

II. MAXWELL MODEL FOR INELASTIC POLAR RODS

At this stage, molecular motors enter the model implicitly by specifying the microscopic interaction rules between two rods. Since the diffusion of small motors is about two order of magnitude higher than that of large and heavy microtubules, in this Section we neglect spatial variations of the motor density and treat the collision rules as spatially homogeneous. Effects of variable motor density are considered in Sec. VI below. Each rod is assumed to be of length l and diameter $d \ll l$, and is characterized by the position of its center of mass \mathbf{r} and orientation angle ϕ .

Consider the orientational dynamics only and ignore the locales of interacting rods (an analog of the Maxwell model of binary collisions in kinetic theory of gases, see e.g. [17]). We model the motor-mediated inelastic interaction by an instantaneous collision in which two rods change their orientations according to the following collision rule:

$$\begin{pmatrix} \phi_1^a \\ \phi_2^a \end{pmatrix} = \begin{pmatrix} \gamma & 1-\gamma \\ 1-\gamma & \gamma \end{pmatrix} \begin{pmatrix} \phi_1^b \\ \phi_2^b \end{pmatrix} \quad (1)$$

where $\phi_{1,2}^b$ are the two rods' orientations before and $\phi_{1,2}^a$ after the collision, and γ characterizes inelasticity of collisions. The angle between two rods is reduced after the collision by a factor $2\gamma - 1$. Totally elastic collision corresponds to $\gamma = 0$ (the rods exchange their angles) and a totally inelastic collision corresponds to $\gamma = 1/2$: rods acquire identical orientation $\phi_{1,2}^a = (\phi_1^b + \phi_2^b)/2$ (see Fig. 1,a). Here we assume that two rods only interact if the angle between them before collision is less than ϕ_0 , $|\phi_2^b - \phi_1^b| < \phi_0 < \pi$. Because of 2π -periodicity, we have to add the rule of collision between two rods with $2\pi - \phi_0 < |\phi_2^b - \phi_1^b| < 2\pi$. In this case we have to replace $\phi_1^{b,a} \rightarrow \phi_1^{b,a} + \pi$, $\phi_2^{b,a} \rightarrow \phi_2^{b,a} - \pi$ in Eq. (1). In the following we will only consider the case of totally inelastic rods ($\gamma = 1/2$) and $\phi_0 = \pi$, the generalization for arbitrary γ and ϕ_0 is straightforward, see Appendix A. The probability $P(\phi)$ obeys the following master equation

$$\begin{aligned} \partial_t P(\phi) = & D_r \partial_\phi^2 P(\phi) + g \int_{C_1} d\phi_1 d\phi_2 P(\phi_1) P(\phi_2) \\ & \times [\delta(\phi - \phi_1/2 - \phi_2/2) - \delta(\phi - \phi_2)] + g \int_{C_2} d\phi_1 d\phi_2 \\ & \times P(\phi_1) P(\phi_2) [\delta(\phi - \phi_1/2 - \phi_2/2 - \pi) - \delta(\phi - \phi_2)] \end{aligned} \quad (2)$$

where g is the “collision rate” proportional to the number density of molecular motors m , the diffusion term $\propto D_r$ describes thermal fluctuations of rod orientations, and the integration domains C_1, C_2 are shown in Fig. 1b. From the dimensional analysis one finds that the collision rate g is of the order of $m D_r S_0$, since $1/D_r$ is the

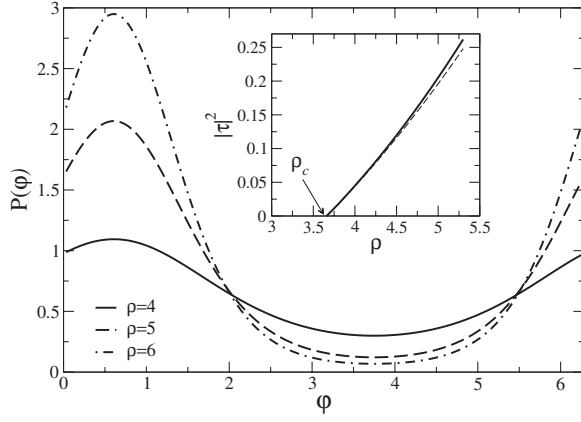


FIG. 2: Stationary solutions $P(\phi)$ for different ρ . Inset: the stationary value of $|\tau|^2$ vs ρ obtained from the Maxwell model (3), dashed line - truncated model (10).

only time scale in Eq. (2), and $S_0 \sim l^2$ is the interaction cross-section of microtubules.

Changing variables $t \rightarrow D_r t$, $P \rightarrow gP/D_r$, $w = \phi_2 - \phi_1$, one obtains

$$\begin{aligned} \partial_t P(\phi) &= \partial_\phi^2 P(\phi) + \int_{-\pi}^{\pi} dw \\ &\times [P(\phi + w/2)P(\phi - w/2) - P(\phi)P(\phi - w)] \end{aligned} \quad (3)$$

The rescaled number density $\rho = \int_0^{2\pi} P(\phi, t) d\phi$ now is proportional to the *density of rods multiplied by the density of motors*. In the following, an increase of the density of molecular motors is reflected in our analysis as an increase of the number density ρ .

A. Orientation instability

Eq. (3) possesses uniform steady-state solution $P(\phi) = P_0 = \rho/2\pi = \text{const}$ corresponding to isotropic distribution of rods. This solution loses its stability with respect to anisotropic perturbations with the increase of density ρ . The instability signals the onset of spontaneous orientation. Substituting solution to Eq. (3) in the form $P(\phi, t) = P_0 + \xi(\phi, t)$, where ξ is small perturbation, we obtain linear equation for ξ :

$$\begin{aligned} \partial_t \xi(\phi) &= \partial_\phi^2 \xi(\phi) + \frac{\rho}{2\pi} \int_{-\pi}^{\pi} (\xi(\phi + w/2) \\ &+ \xi(\phi - w/2) - \xi(\phi - w) - \xi(\phi)) dw \end{aligned} \quad (4)$$

Looking for the solution to Eq. (4) in the form $\xi \sim \exp[\lambda_k t \pm ik\phi]$, where $k \neq 0$ is integer, for the growth rate λ_k we find

$$\lambda_k = \rho \left(\frac{4}{k\pi} \sin(\pi k/2) - 1 \right) - k^2 \quad (5)$$

Thus, it follows from Eq. (5) that perturbations with $k = \pm 1$ have the largest growth rate $\lambda_1 = \rho(4/\pi - 1) - 1$.

The instability ($\lambda_1 > 0$) occurs for the density $\rho > \rho_c = \pi/(4 - \pi) \approx 3.662$, and leads to breaking the azimuthal symmetry and formation of anisotropic, i.e. oriented states. The resulting orientation is determined by initial conditions contained in the perturbation ξ .

B. Fourier expansion

Let us consider the Fourier harmonics of the probability density $P(\phi)$:

$$P_k = \langle e^{-ik\phi} \rangle = \frac{1}{2\pi} \int_0^{2\pi} d\phi e^{-ik\phi} P(\phi, t) \quad (6)$$

The zeroth harmonic $P_0 = \rho/2\pi = \text{const}$, and the real and imaginary parts of P_1 represent the components $\tau_x = \langle \cos \phi \rangle$, $\tau_y = \langle \sin \phi \rangle$ of the average orientation vector τ , $\tau_x + i\tau_y = P_1^*$. Substituting (6) into Eq.(3) yields:

$$\dot{P}_k + (k^2 + \rho)P_k = 2\pi \sum_m P_{k-m} P_m S[\pi k/2 - m\pi] \quad (7)$$

(here $S(x) = \sin x/x$). Due to the rotational diffusion term, the magnitudes of high-order harmonics decay exponentially with $|k|$, see Eq. (5). Neglecting all P_k for $|k| > 2$ we obtain from Eq.(7)

$$\dot{P}_1 + P_1 = P_0 P_2 (4 - \pi) - \frac{8}{3} P_2 P_1^* \quad (8)$$

$$\dot{P}_2 + 4P_2 = -P_0 P_2 2\pi + 2\pi P_1^2 \quad (9)$$

Since near the instability threshold the decay rate of P_2 is much larger than the growth rate of P_1 , see Eq. (5), we can neglect the time derivative \dot{P}_2 and obtain $P_2 = AP_1^2$ with $A = 2\pi(\rho + 4)^{-1}$ and arrive at:

$$\dot{\tau} = \epsilon \tau - A_0 |\tau|^2 \tau \quad (10)$$

with

$$\begin{aligned} \epsilon &= \rho(4\pi^{-1} - 1) - 1 \approx 0.273\rho - 1 \\ A_0 &= 8A/3 = \frac{16\pi}{3(\rho + 4)} \end{aligned} \quad (11)$$

For large enough $\rho > \rho_c = 3.662$, an ordering instability leads to spontaneous rods alignment. This instability saturates at the value determined by ρ . Close to the threshold $A_0 \approx 2.18$.

In order to verify our approximations we solved Eq. (3) for $\gamma = 1/2$, $\phi_0 = \pi$ numerically by the finite difference method. We find that random initial conditions rapidly evolved towards a single-peaked stationary distribution, the position of the maximum of the distribution being determined by initial conditions. Fig. 2 shows typical stationary solutions $P(\phi)$ obtained from Eq. (3) for different values of ρ . One sees that $P(\phi)$ is weakly non-uniform near the critical density, and becomes more peaked with the increase of the density. From the numerically obtained distribution we extracted orientation

amplitude $|\tau|$ and compared it with the analytical result $|\tau|^2 = \epsilon/A_0$ from Eqs. (10),(11). As seen in the Inset, the corresponding values of $|\tau|$ are consistent with the truncated model (10) up to $\rho < 5.5$.

We also studied Eq. (3) for $\phi_0 < \pi$. Whereas for ϕ_0 close to π no qualitative difference was found, for smaller ϕ_0 , e.g. $\phi_0 < \pi/2$ we often obtained long-living multiple peak distributions, with the number of peaks roughly π/ϕ_0 . While the distribution possibly relaxes towards a single peak, the transient time appears to be very large due to exponentially weak interaction between the peaks.

III. MICROSCOPIC PICTURE OF TUBULE-TUBULE INTERACTION

In order to generalize our model to account for spatial localization of interaction between tubules, we need to introduce a more specific model of interaction between two tubules mediated by a molecular motor. Namely, we should specify the “collision rules”, or a relationship between positions and orientations of two tubules before and after the interaction via motor attachment/detachment, and the “collision rate”, or the probability of the collision to occur given the positions and orientations of two tubules. The latter will play a role of interaction kernel in the corresponding master equation for the tubule probability distribution.

A. Collision rules

Here we specify these rules by integrating the equations of motion of the two tubules. This calculation is based on a number of simplifications. We assume that two infinitely rigid rods of equal length l interact with one molecular motor. We assume that the motor moves with constant speed V along the rods (the results can be trivially generalized for the case of $V \neq \text{const}$). To simplify the system even further, we consider a symmetric case: the distance of the motor from the center point of the rod S , $-l/2 < S < l/2$ is the same for both rods, see Figure 3. Since the size of a motor (≈ 30 nm) is much smaller than the length of a microtubule (5..10 micron), we consider a limit of zero motor size. Since the motor’s bending elasticity is rather small, we approximate the motor by a soft spring and prescribe that the force F exerted on the tubules due to motor motion is perpendicular to the bisector of the angle between the tubules (i.e. along the x -axis, see Fig. 3. Even if the symmetry is initially broken, and the force is exerted at an angle to the x -axis, the force will initiate a relative displacement of the tubules in the y direction which will shift the binding points in such a way as to restore the symmetry.

The equations governing evolution of the angle ϕ between the microtubule and the bisector and the coordinates X, Y of the center of mass of the microtubule are

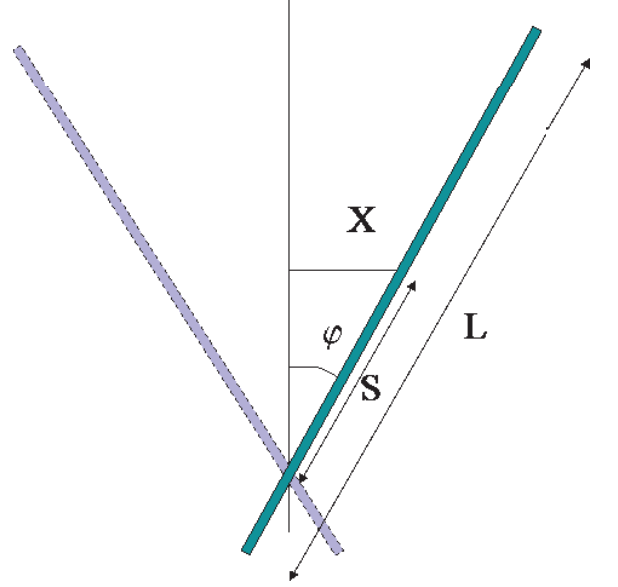


FIG. 3: Sketch of the interaction of two microtubules

obtained from balance of torques and forces due to motor motion and viscous drag forces

$$\partial_t \phi = \xi_r^{-1} S \cos(\phi) F \quad (12)$$

$$\partial_t X = (\xi_{\parallel}^{-1} \cos^2 \phi + \xi_{\perp}^{-1} \sin^2 \phi) F, \quad (13)$$

$$\partial_t Y = (\xi_{\parallel}^{-1} - \xi_{\perp}^{-1}) \sin \phi \cos \phi F \quad (14)$$

Here $\xi_r, \xi_{\parallel}, \xi_{\perp}$ are rotational and translational viscous drag coefficients, see Eq. (55) below. In the following we neglect the anisotropy of the translation friction ($\xi_{\parallel} = \xi_{\perp}$ [18]), then the equations will simplify considerably

$$\partial_t \phi = \xi_r^{-1} S \cos(\phi) F \quad (15)$$

$$\partial_t X = \xi_{\parallel}^{-1} F, \quad (16)$$

$$\partial_t Y = 0. \quad (17)$$

Additional kinematic equation is obtained from the condition that the motor is attached at the distance S from the center of tubule, which gives

$$X = -S \sin \phi \quad (18)$$

Differentiating Eq. (18) with time and using $dS/dt = V$, we exclude F and derive an equation for ϕ (note that the analysis in this Section is also valid for arbitrary time-dependent velocity of the motor $V(t) > 0$)

$$\frac{d\phi}{dt} = -\frac{kVS \cos(\phi) \sin(\phi)}{1 + kS^2 \cos^2(\phi)} \quad (19)$$

where $k = \xi_{\parallel}/\xi_r \approx 12/l^2$, see Eq. (55). We make the following substitutions:

$$\tau \rightarrow kS^2; u \rightarrow \cos(\phi)^2 \quad (20)$$

In new variables Eq (19) can be written as

$$\frac{d\tau}{du} = \frac{1 + \tau u}{u(1 - u)} \quad (21)$$

Eq. (21) is linear with respect to τ and therefore has an exact solution

$$\tau = \frac{C + \log(u)}{1 - u} \quad (22)$$

where C is a constant determined by initial conditions. Returning to original variables, we obtain

$$\frac{C + \log(\cos^2(\phi))}{\sin(\phi)^2} = kS^2 \quad (23)$$

For small angles ϕ Eq. (23) simplifies and we obtain

$$\phi = \phi_0 \frac{\sqrt{1 + kS_0^2}}{\sqrt{1 + kS^2}} \quad (24)$$

where ϕ_0 and S_0 are the initial conditions at $t = 0$.

For the final angle obtained when the motor reaches the end of the microtubules ($S = l/2$) we obtain

$$\tilde{\phi} = \phi_0 \frac{\sqrt{1 + kS_0^2}}{\sqrt{1 + kl^2/4}} \quad (25)$$

As one sees from Eq. (25), the final angle $\tilde{\phi}$ depends on the initial angle ϕ_0 and the initial attachment position S_0 . Assuming that the probability of attachment of the motor is independent of the position along the microtubule S , in the small angle approximation for average angle

$$\langle \tilde{\phi} \rangle = l^{-1} \int_{-l/2}^{l/2} \tilde{\phi}(S_0) dS_0 \quad (26)$$

we obtain

$$\langle \tilde{\phi} \rangle = \phi_0 \left[\frac{1}{2} + \frac{\text{asinh}(\sqrt{kl^2}/2)}{\sqrt{kl^2} \sqrt{1 + kl^2/4}} \right] \quad (27)$$

Thus, the averaged change in the angle $\epsilon = \langle \phi \rangle / \phi_0$ is

$$\epsilon = \frac{1}{2} + \frac{\text{asinh}(\sqrt{kl^2}/2)}{\sqrt{kl^2} \sqrt{1 + kl^2/4}} \quad (28)$$

Obviously, for $kl^2 \rightarrow \infty$ the relative angle change $\epsilon \rightarrow 1/2$. Correspondingly, the restitution coefficient $\gamma = (1 - \epsilon)/2 \rightarrow 1/4$, in agreement with our assumptions on inelastic collision between the rods. For the case of rigid rods we obtain from Eq. (55) that $kl^2 \approx 12$, which gives $\epsilon \approx 0.67$, or $\gamma \approx 0.17$, which is considerably smaller than fully-inelastic case of $\gamma = 1/2$. With the increase of k the coefficient γ increase, e.g. for $k = 30$ one obtains $\gamma = 0.2$.

For arbitrary ϕ_0 , in order to find the average angle change we solved Eq. (23),(26) numerically (see Fig. 4). There is a very weak dependence of γ on the initial angle ϕ . In a wide range of angles $\Delta\phi < 0.75\pi$, parameter $\gamma \approx 0.2$ and then $\gamma \rightarrow 0$ for $\phi \rightarrow \pi$.

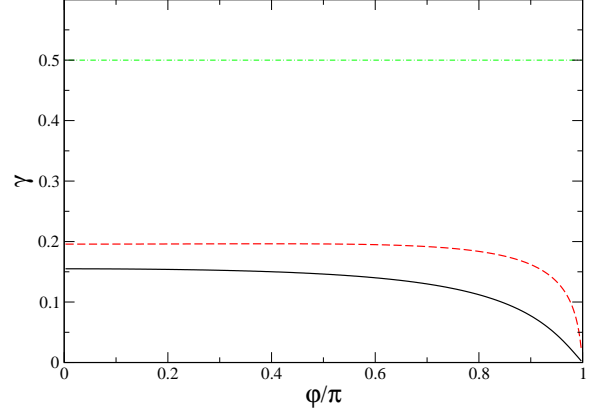


FIG. 4: The effective restitution coefficient γ calculated from Eq. (26) for $k = 12$ (solid line). For comparison γ at $k = 30$ is also shown (dashed line). Dot-dashed line indicates the limit of fully inelastic interaction $\gamma = 0.5$.

B. Collision rate

Now we turn to the calculation of the collision rate $W(\mathbf{r}_1, \mathbf{r}_2, \phi_1, \phi_2)$ between two tubules with center-of-mass positions $\mathbf{r}_1, \mathbf{r}_2$ and orientation angles ϕ_1, ϕ_2 . We consider a translationally and rotationally invariant system, so the collision rate depends only on the position and orientation differences, $W(\mathbf{r}, \phi)$, where $\mathbf{r} = \mathbf{r}_1 - \mathbf{r}_2$, and, as before, $\phi = (\phi_1 - \phi_2)/2$.

Microtubules interact via a motor attachment only if they intersect, which is expressed by the condition

$$|\mathbf{r}_1 - \mathbf{r}_2| < \frac{l}{2} \sin \phi \quad (29)$$

This gives the collision rate in the form

$$W = g\Theta(|\mathbf{r}_1 - \mathbf{r}_2| - l/2 \sin \phi) \quad (30)$$

where Θ is the Θ -function, and g is the probability of a motor to bind to both tubules given that they intersect. The latter is directly proportional to the concentration of molecular motors bound to a tubule. If the concentration of the motors along the tubules were uniform, the collision rate would be uniform inside the parallelogram defined by Eq.(30). However, due to the transport of motors along the tubules, their concentrations increase towards the polar ends of the filaments.

In order to compute the inhomogeneous motor distribution along a filament, we assume that the motors can be in two different states, bound and free. The concentration of free motors m_f is a function of the coordinate along the tubule S , ($-l/2 < S < l/2$), perpendicular coordinate r_\perp (we consider a two-dimensional domain), and time t . Bound motors are localized on the tubule itself, so their concentration is $M_b(S, t)\delta(r_\perp)$.

The inhomogeneous motor distribution can be evaluated from the following microscopic equations for motor attachment/detachment and advection processes:

$$\begin{aligned}\partial_t m_f &= (p_{off} M_b - p_{on} m_f) \delta(r_\perp) + D \nabla^2 m_f \\ \partial_t M_b &= -p_{off} M_b + p_{on} m_f(S, 0, t) - \partial_S (V M_b)\end{aligned}\quad (31)$$

These equations, formulated in terms of the concentration of bound/free motors M_b, m_f , describe random binding/unbinding of the motors with the probabilities $p_{on, off}$; diffusion of free motors (diffusion coefficient D), and the advection of bound motors with the velocity V along the tubule. The parameter p_{off} characterizes processivity of molecular motors: large p_{off} corresponds to small processivity, motor unbinds soon after it binds to a filament.

According to experiments (see e.g. [19]), while multiple motors can be attached to a single tubule, only one motor can be attached per elementary binding site (which represents a section of approximately $l_0 = 10$ nm along the tubule). This leads to a kind of hard-core repulsion which in the simplest approximation can be taken into account by introducing local “pressure” P of bound motors, and modifying the transport speed V ,

$$V = V_0 - \eta \partial_S P \quad (32)$$

where η is an effective mobility. Pressure P diverges as the bound motor density approaches densely packed limit of one motor per binding site $M_b \rightarrow M_0 \sim 1/l_0$. We will adopt a simple generic expression for the pressure as a function of the bound motor density (see for comparison expressions for pressure in granular hydrodynamics near closed-packed density [20, 21, 22])

$$P = \frac{M_b T}{1 - M_b/M_0} \quad (33)$$

The “temperature” T is determined by fluctuations of bound motors on the tubule and is typically small, so the pressure can be neglected everywhere except where the density is very close to the dense limit.

In the stationary state Eqs. (32) assume the form

$$\begin{aligned}(p_{off} M_b - p_{on} m_f) \delta(r_\perp) + D \nabla^2 m_f &= 0 \\ -p_{off} M_b + p_{on} m_f(S, 0) &= \partial_S [V_0 M_b - \eta M_b \partial_S P]\end{aligned}\quad (34)$$

Since the diffusion constant D of free motors is large, we can neglect the inhomogeneity in the free motor distribution and assume $m_f = \text{const}$ in Eq.(35). Eq. (35) has to be solved with the boundary condition $M_b = 0$ at $S = -l/2$. At the end of the tubule $S = l/2$ the “exit” flux of bound motors $V M_b$ is determined by the detachment probability p_{end} of the motor, resulting in the condition $V M_b = p_{end} l_0 M_b$. For small T , the density of bound motors has two distinct phases: low-density “gas phase” near the beginning of the tubule ($S = -l/2$), and a high density “solid phase” near the end ($S = l/2$) [23]. The location of the boundary between these phases

can be found by equating the fluxes of bound motors in the two phases. In the low density phase, the pressure term can be neglected due to small T , and the solution has the form

$$M_b = \frac{p_{on} m_f}{p_{off}} \left[1 - \exp \left(-\frac{p_{off}}{V_0} (S + l/2) \right) \right] \quad (36)$$

Typically, $p_{off} V_0^{-1} l \gg 1$, so the density saturates very quickly to the equilibrium value $M_e = p_{on} p_{off}^{-1} m_f$. This solution corresponds to a constant flux of motors along the tubule,

$$F_1 = V_0 M_e = \frac{V_0 p_{on} m_f}{p_{off}} \quad (37)$$

In the solid phase at a very low temperature T , the motor density is very close to M_0 . Thus, at the end of the tubule, the flux of motors is equal to the number of motors leaving the tubule in a unit time $p_{end} M_0$. According to Eq.(35), the flux of motors in the solid phase is a linear function of the coordinate,

$$F_2 = p_{end} l_0 M_0 + [p_{off} M_0 - p_{on} m_f] (l/2 - S) \quad (38)$$

The two phases are separated by a narrow interface (the width of the interface vanishes when $T \rightarrow 0$) whose position S_0 is determined by equating these two fluxes, $F_1 = F_2$,

$$\frac{V_0 p_{on} m_f}{p_{off}} = p_{end} l_0 M_0 + [p_{off} M_0 - p_{on} m_f] (l/2 - S_0) \quad (39)$$

This yields the following expression for the interface position

$$S_0 = \frac{l}{2} + \frac{p_{end} l_0 M_0 - V_0 p_{on} p_{off}^{-1} m_f}{p_{off} M_0 - p_{on} m_f} \quad (40)$$

Obviously, S_0 grows with p_{end} , and at $p_{end} = V_0 p_{on} m_f [p_{off} l_0 M_0]^{-1}$, we obtain $S_0 = l/2$, i.e. the solid phase disappears.

Thus, the bound motor density M_b is approximately described by the following step function

$$M_b(S) \approx M_e + (M_0 - M_e) \Theta(S - S_0) \quad (41)$$

The inhomogeneous distribution of bound motors directly leads to the anisotropy of the collision rate. The coordinates along the microtubules $S_{1,2}$ are related to the positions $\mathbf{r}_{1,2}$ of the center of microtubules as follows

$$S_{1,2} = \mathbf{n}_{1,2} \cdot (\mathbf{r} - \mathbf{r}_{1,2}) \quad (42)$$

The collision rate is proportional to the sum of the bound motor concentration times the cross-linking rate g_0 ,

$$g = g_0 [M_b(S_1^0) + M_b(S_2^0)] \quad (43)$$

where $S_{1,2}^0$ are the values of $S_{1,2}$ at the intersection point. Excluding \mathbf{r} from Eq. (42) one obtains

$$\begin{aligned} S_1^0 &= \frac{(\mathbf{r}_1 - \mathbf{r}_2)(\mathbf{n}_2 - \mathbf{n}_1(\mathbf{n}_1\mathbf{n}_2))}{1 - (\mathbf{n}_1\mathbf{n}_2)^2} \\ S_2^0 &= -\frac{(\mathbf{r}_1 - \mathbf{r}_2)(\mathbf{n}_1 - \mathbf{n}_2(\mathbf{n}_1\mathbf{n}_2))}{1 - (\mathbf{n}_1\mathbf{n}_2)^2} \end{aligned} \quad (44)$$

Non-uniform $M_b(S)$ produce anisotropy: $g(\mathbf{r}_1, \mathbf{n}_1, \mathbf{r}_2, \mathbf{n}_2) \neq g(\mathbf{r}_1, \mathbf{n}_2, \mathbf{r}_2, \mathbf{n}_1)$. However, the collision rate Eq. (43) with the step-wise expressions for $S_{1,2}^0$ (41) is awkward and impractical for further calculations. In the subsequent section we will not use the exact form (30) with Eq.(43) as a kernel in the master equation, but replace it with a more simple form which nevertheless retains the main features of (30),(43), namely, localization and anisotropy,

$$W \approx W_0(\mathbf{r}_1 - \mathbf{r}_2)(1 - \beta l^{-1}(\mathbf{r}_1 - \mathbf{r}_2)(\mathbf{n}_1 - \mathbf{n}_2)) \quad (45)$$

where the symmetric part of the kernel W_0 is of the Gaussian form

$$W_0(\mathbf{r}) = \frac{g_0}{\pi b^2} \exp[-\mathbf{r}^2/b^2] \quad (46)$$

with the spatial scale $b \approx l/2$. The dimensionless parameter β characterized the collision rate anisotropy. The interaction kernel in this form was proposed by us on the symmetry grounds in Ref. [15].

While the form (45) cannot be rigorously derived from (30),(43), the anisotropy coefficient β as a function of kinetic parameters can be estimated from the expression (41). First of all, we approximate the step function in Eq. (41) by the linear function

$$M_b(S) \approx \bar{M} + \bar{\alpha}S \quad (47)$$

where the mean density \bar{M} and mean slope $\bar{\alpha}$ are calculated by the least mean square method using Eq. (41),

$$\begin{aligned} \bar{M} &= \frac{1}{l} \int_{-l/2}^{l/2} M_b dS = \frac{M_0 + M_e}{2} + (M_0 - M_e) \frac{S_0}{l} \\ \bar{\alpha} &= \frac{12}{l^3} \int_{-l/2}^{l/2} M_b S dS = 6 \frac{M_0 - M_e}{l^3} \left(\frac{l^2}{4} - S_0^2 \right) \end{aligned} \quad (48)$$

To evaluate the effective kernel we substitute Eq. (47) into Eq. (43) and using relations (44), obtain

$$\begin{aligned} g &\approx g_0 [2\bar{M} + \bar{\alpha}(S_1^0 + S_2^0)] \\ &= g_0 \left(2\bar{M} - \bar{\alpha} \frac{(\mathbf{r}_1 - \mathbf{r}_2)(\mathbf{n}_1 - \mathbf{n}_2)}{1 - \mathbf{n}_1\mathbf{n}_2} \right) \end{aligned} \quad (49)$$

As one sees from Eq. (49), it coincides with phenomenological kernel Eq. (45) up to the factor $(1 - \mathbf{n}_1\mathbf{n}_2)$ in denominator. The value of the dimensionless kernel anisotropy is then

$$\beta = \frac{\bar{\alpha}l}{2\bar{M}} \quad (50)$$

Assuming that the density in the solid phase M_0 is much larger than the density in the gas phase M_e , $\mu = M_0/M_e \gg 1$, we obtain the following estimate for the anisotropy β for $p_{end} \rightarrow 0$:

$$\beta \approx 3 \left(\frac{1}{2} - \frac{S_0}{l} \right) = 3 \frac{V_0 - p_{end}\mu l_0}{lp_{off}\mu}. \quad (51)$$

The anisotropy is maximum for $p_{end} = 0$, ($\beta \approx V_0/p_{off}l\mu$), decreases with the increase of p_{end} and vanishes (at this approximation) at $p_{end} = V_0/\mu l_0$.

We can estimate the parameter β for different type of motors using the data from Ref. [4, 5]. The parameters for kinesin and NCD are: $V = 1 \mu/sec$, $p_{on} = 20 sec^{-1}$, $p_{off} = 0.5 sec^{-1}$, and $p_{end} = 70 sec^{-1}$ for kinesin and $p_{end} = 2.5 sec^{-1}$ for NCD. Projected (two-dimensional) density of free motors m_f in Refs. [4, 5] was taken $m_f = 0.05 - 2 \mu m^{-2}$. For the linear density of bound motors we obtain $M_e = p_{on}m_f d_0/p_{off}$ and $M_0 = 1/l_0$, where $d_0 \approx 2l_0$ is the diameter of microtubule. For parameter μ obtain $\mu = M_0/M_e = p_{off}/(d_0 l_0 p_{on} m_f) \approx 10..500 \gg 1$. Thus, for NCD-like motors when $l_0 \mu p_{end} \ll 1$ we obtain the anisotropy parameter β (depending on the density ratios μ)

$$\beta_{NCD} \approx \frac{3V_0}{lp_{off}\mu} \approx 10^{-3}..10^{-1} \quad (52)$$

It follows from Eq. (52) that the kernel anisotropy increases with the increase of the concentration of free motors. Correspondingly, since for kinesin parameters $p_{end} > V_0 p_{on} m_f [p_{off} l_0 M_0]^{-1}$ and no solid phase is formed, the anisotropy coefficient β is essentially zero.

In this Section we considered only one mechanism contributing to the kernel anisotropy: inhomogeneous distribution of bound motors. Possibly there are other mechanisms affecting the anisotropy of the interaction, for example, finite bending rigidity of the microtubules may also contribute to both the collision rules and the collision rate. However we leave this interesting topic to further studies.

IV. SPATIAL LOCALIZATION OF TUBULE-TUBULE INTERACTION

To describe the *spatial localization* of tubule-tubule interaction we introduce the probability distribution $P(\mathbf{r}, \phi, \mathbf{t})$ to find a rod with orientation ϕ at location \mathbf{r} at time t . The master equation for $P(\mathbf{r}, \phi, t)$ can be written as

$$\begin{aligned} \partial_t P(\mathbf{r}, \phi) = & \partial_\phi^2 P(\mathbf{r}, \phi) + \partial_i D_{ij} \partial_j P(\mathbf{r}, \phi) + \int \int d\mathbf{r}_1 d\mathbf{r}_2 \int_{-\phi_0}^{\phi_0} dw [W(\mathbf{r}_1, \mathbf{r}_2, \phi + w/2, \phi - w/2) \\ & \times P(\mathbf{r}_1, \phi + w/2) P(\mathbf{r}_2, \phi - w/2) \delta\left(\frac{\mathbf{r}_1 + \mathbf{r}_2}{2} - \mathbf{r}\right) - W(\mathbf{r}_1, \mathbf{r}_2, \phi, \phi - w) P(\mathbf{r}_2, \phi) P(\mathbf{r}_1, \phi - w) \delta(\mathbf{r}_2 - \mathbf{r})] \end{aligned} \quad (53)$$

where we performed the same rescaling as in Eq.(3) using g_0 instead of g and dropped argument t for brevity. We normalized the probability $P \rightarrow P/l^2$.

Unlike the Maxwell model equation (3), Eq. (53) contains two diffusion terms (translational and angular), and the motor-mediated tubule-tubule collision integral now contains an interaction kernel which depends on the relative tubule positions and orientations. The angular diffusion coefficient D_r and the translational diffusion tensor D_{ij} are known from the polymer physics [24]:

$$\begin{aligned} D_{ij} &= \frac{1}{D_r} (D_{\parallel} n_i n_j + D_{\perp} (\delta_{ij} - n_i n_j)) \\ D_{\parallel} &= \frac{k_B T}{\xi_{\parallel}}, \\ D_{\perp} &= \frac{k_B T}{\xi_{\perp}}, \\ D_r &= \frac{4k_B T}{\xi_r} \end{aligned} \quad (54)$$

where $\xi_{\parallel}, \xi_{\perp}, \xi_r$ are corresponding viscous drag coefficients. For rigid rod-like molecules,

$$\xi_{\parallel} = \frac{2\pi\eta_s l}{\log(l/d)}; \quad \xi_{\perp} = 2\xi_{\parallel}; \quad \xi_r \approx \frac{\pi\eta_s l^3}{3 \log(l/d)} \quad (55)$$

where η_s is shear viscosity [24]. Since we scaled time by the rotational diffusion time $t \rightarrow D_r t$, in new variables

the translational diffusions assume a very simple form: $D_{\parallel} = 1/24, D_{\perp} = 1/48$, see Eq. (54). Note that the drag coefficients are slightly modified for thin films and membranes, see e.g [25].

The last term of Eq.(53) describes motors-mediated interaction of rods. While the results of the previous section indicate that the angular “inelasticity coefficient” γ is less than $1/2$, we postulate here that after the interaction, the two rods acquire the same orientation, $\phi = (\phi_1 + \phi_2)$ and the same spatial location in the middle of their original locations, $\mathbf{r} = (\mathbf{r}_1 + \mathbf{r}_2)/2$. These assumptions are made to simplify the calculations and final equations, however generalization to arbitrary collision inelasticity is straightforward (see Appendix A).

A. Continuum equations

After integration over the δ functions Eq. (53) assumes the form

$$\frac{\partial P}{\partial t} = \frac{\partial^2 P}{\partial \phi^2} + \partial_i D_{ij} \partial_j P + Z_0 + \beta Z_1 \quad (56)$$

where nonlinear terms

$$\begin{aligned} Z_0 &= \int d\mathbf{r}_1 \int_{-\phi_0}^{\phi_0} dw [2W_0(2(\mathbf{r}_1 - \mathbf{r})) P(\mathbf{r}_1, \phi + w\gamma, t) P(2\mathbf{r} - \mathbf{r}_1, \phi + w(\gamma - 1), t) \\ &\quad - W_0(\mathbf{r}_1 - \mathbf{r}) P(\mathbf{r}, \phi, t) P(\mathbf{r}_1, \phi - w, t)] \end{aligned} \quad (57)$$

and

$$\begin{aligned} Z_1 &= \int d\mathbf{r}_1 \int_{-\phi_0}^{\phi_0} dw [2W_0(2(\mathbf{r}_1 - \mathbf{r})) (\mathbf{r}_1 - \mathbf{r}) \cdot (\mathbf{n}_1 - \mathbf{n}) P(\mathbf{r}_1, \phi + w\gamma, t) P(2\mathbf{r} - \mathbf{r}_1, \phi + w(\gamma - 1), t) \\ &\quad - W_0(\mathbf{r}_1 - \mathbf{r}) (\mathbf{r}_1 - \mathbf{r}) \cdot (\mathbf{n}_1 - \mathbf{n}) P(\mathbf{r}, \phi, t) P(\mathbf{r}_1, \phi - w, t)] \end{aligned} \quad (58)$$

are generated by the collision integral in Eq. (53).

To proceed, we again perform the Fourier expansion of the probability distributions in ϕ and truncate the series at $|n| > 2$. Now $2\pi P_0$ gives the local number density

$\rho(\mathbf{r}, t)$, and $P_{\pm 1}$ the local orientation $\boldsymbol{\tau}(\mathbf{r}, t)$. The integration of the diffusion term in Eq.(56) generates linear terms, and the nonlinear terms Z_0, Z_1 (see Appendix B) produce nonlinear terms in the corresponding equations

for ρ, τ .

After rescaling space by l , and introducing dimensionless parameters $B = b/l$ characterizing the width of the interaction kernel and $H = \beta B^2$ characterizing normal-

ized strength of anisotropy of interaction, we arrive at the set of equations for coarse-grained local density ρ and orientation τ

$$\partial_t \rho = \nabla^2 \left[\frac{\rho}{32} - \frac{B^2 \rho^2}{16} \right] - \frac{\pi B^2 H}{16} [3 \nabla \cdot (\tau \nabla^2 \rho - \rho \nabla^2 \tau) + 2 \partial_i (\partial_j \rho \partial_j \tau_i - \partial_i \rho \partial_j \tau_j)] - \frac{7 \rho_0 B^4}{256} \nabla^4 \rho \quad (59)$$

$$\partial_t \tau = \frac{5}{192} \nabla^2 \tau + \frac{1}{96} \nabla (\nabla \cdot \tau) + \epsilon \tau - A_0 |\tau|^2 \tau - H \left[\frac{\nabla \rho^2}{16\pi} - \left(\pi - \frac{8}{3} \right) \tau (\nabla \cdot \tau) - \frac{8}{3} (\tau \nabla) \tau \right] + \frac{B^2 \rho_0}{4\pi} \nabla^2 \tau \quad (60)$$

These equations generalize Eq.(10) for the case of spatially localized coupling. For simplicity the last two terms in Eqs. (59),(60) have been linearized near the mean density $\rho_0 = \langle \rho \rangle$, otherwise more complicated expressions given in Appendix B are needed. This approximation is justified by the fact that in the relevant range of parameters B, H the density variations are small compared to the variations of the orientation τ . The last term in Eq. (59) regularizes the short-wave instability when the diffusion term changes sign for $\rho_0 > \rho_b = 1/4B^2$. This instability leads to strong density variations associated with formation of dense microtubule bundles (see Figs. 6, 8 below) which is also observed experimentally for large density of molecular motors.

B. Stability of Asters and Vortices

If $B^2 H \ll 1$, the density modulations are rather small, and Eq. (60) for orientation τ decouples from Eq. (59). It is convenient to rewrite Eq. (60) for complex variable $\psi = \tau_x + i\tau_y$:

$$\partial_t \psi = \epsilon \psi - A_0 |\psi|^2 \psi + D_1 \nabla^2 \psi + D_2 \bar{\nabla}^2 \psi^* + H \left(\left(\pi - \frac{8}{3} \right) \psi \text{Re} \bar{\nabla} \psi^* + \frac{8}{3} (\text{Re} \psi^* \bar{\nabla}) \psi \right) \quad (61)$$

where operator $\bar{\nabla} = \partial_x + i\partial_y$, $D_1 = 1/32 + \rho_0 B^2/4\pi$, $D_2 = 1/192$. Eq. (61) is similar to generalized Ginzburg-Landau equation known in the context of superconductivity, superfluidity, nonlinear optics, and pattern formation, see e.g. [27]. Let us focus on the structure and the dynamics of radially-symmetric solutions of (61) which can be sought in polar coordinates r, θ in the following generic form:

$$\psi = \sqrt{A_0/\epsilon} A(r) \exp(i\theta) \quad (62)$$

where the complex amplitude $A(r) = \Phi(r) \exp[i\varphi(r)]$, and the phase $\varphi(r)$ is a real function. The solution $\varphi(r) = 0, \pi$ corresponds to asters, and the solution with $\varphi(r) \neq 0$ describes vortices, see Fig. 5. Transitions between asters and vortices can be examined in the frame-

work of a one-dimensional problem for the complex variable $A(r)$,

$$\partial_t A = D_1 \Delta_r A + D_2 \Delta_r A^* + (1 - |A|^2) A + H \left(a_1 A \text{Re} \nabla_r A + a_2 \partial_r A \text{Re} A + \frac{ia_2 A \text{Im} A}{r} \right) \quad (63)$$

with the following differential operators

$$\Delta_r = \partial_r^2 + r^{-1} \partial_r - r^{-2}; \nabla_r = \partial_r + r^{-1} \quad (64)$$

and parameters

$$a_1 = (\pi - 8/3)/\sqrt{A_0} \approx 0.321, a_2 = 8/3\sqrt{A_0} \approx 1.81$$

Here we rescaled time $t \rightarrow t/\epsilon$ and space variable by $r \rightarrow r/\sqrt{\epsilon}$.

The aster and vortex solutions obtained by numerical integration of Eq. (63) for certain parameter values are shown in Fig. 7. Vortices exist only for small values of H and give way to asters for larger H or larger ρ . For $H = 0$, Eq.(63) reduces to a form which was studied in [26]. It was shown in [26] that the term $\Delta_r A^*$ favors vortex solution ($\varphi = \pm\pi/2$). In contrast, terms proportional to H select asters with $\varphi = \pi$ (aster for $\varphi = 0$ is unstable for the anisotropy parameter $H > 0$). Note that $\varphi = \pi$ corresponds to asters with the direction of arrows towards the center, as it is shown in Fig. 5. Since we associated the direction of the vector τ with the direction of motion of molecular motors along the microtubules, the aster with $\varphi = \pi$ corresponds to the experimental situation: motor moves towards the center of the aster. Increasing H leads to gradual reduction of φ , and at a finite $H_0(\rho_0)$, $\phi(r) = \pi$, i.e. the transition from vortices to asters occurs. For $0 < H < H_0$, the vortex solution has a non-trivial structure. As seen in Fig. 7, the phase $\varphi \rightarrow \pi$ for $r \rightarrow \infty$, i.e. vortices and asters become indistinguishable far away from the core.

The transitions between asters and vortices can be studied in the framework of linearized Eq. (63). For this purpose the solution to Eq. (63) can be sought in the form

$$A(r) = \Phi(r) + iw(r) \exp(i\lambda t) \quad (65)$$

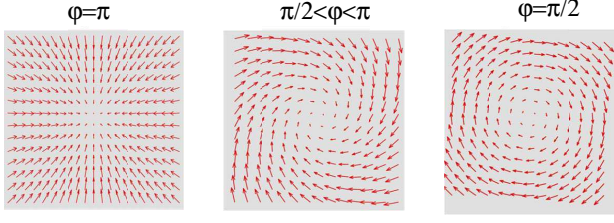


FIG. 5: Schematic representation of orientation fields τ for three different values of φ : aster ($\varphi = \pi$); generic vortex ($\pi/2 < \varphi < \pi$) and ideal vortex ($\varphi = \pm\pi/2$).

where small real perturbation w obeys a linear equation $\hat{L} = \lambda w$ with operator

$$\hat{L} \equiv \bar{D}\Delta_r + (1 - \Phi^2 + a_1 H \nabla_r \Phi) + a_2 H \Phi \nabla_r \quad (66)$$

($\bar{D} = D_1 - D_2$) with zero boundary conditions at $r = 0, \infty$. This eigenvalue problem can be solved by the matching-shooting method. A positive eigenvalue λ corresponds to the emergence of a non-zero phase $\phi(r)$, i.e. a vortex.

The resulting phase diagram of the continuum model (59), (60) is shown in Fig. 6. The solid line $H_0(\rho_0)$ separating vortices from asters is obtained from the solution of the linearized Eq. (63) by tracking the most unstable eigenvalue λ of the aster. The dashed line corresponds to the onset of the orientation instability, $\rho_0 = \rho_c$. The lines meet at the critical point $H_c = H_0(\rho_c)$ above which vortices are unstable for arbitrary small $\epsilon > 0$. The phase diagram is qualitatively consistent with experiments, see Ref. [5]: for low value of kernel anisotropy $H < H_c$ (which according to our estimates in Sec. IIIB correspond to kinesin-like motors with very small anisotropy value β) increase of the density ρ_0 first leads to formation of vortices and then asters. For $H > H_c$ (which apparently correspond to Ncd motors with large anisotropy) only asters are observed. For large density values in addition to orientation instability one observes density instability $\rho_0 > \rho_b = 1/4B^2$ produced by Eq. (59) when the diffusion term changes sign. Numerical studies of the full system (59), (60) indeed indicate formation of extended domains of high density not associated with the asters, see Fig. 8. While our model (59), (60) yields the density instability and bundle formation in accordance with experiment, we anticipate only qualitative agreement in this regime because the model itself is derived in the low density limit when only binary interactions are included.

C. Interaction of asters and vortices

For $H \neq 0$ well-separated vortices and asters exhibit exponentially weak interaction. For asters it follows from the fact that \hat{L} is not a self-adjoint operator. To investigate the interaction between asters we need to examine the asymptotic null-space of the adjoint operator \hat{L}^\dagger for $r \rightarrow \infty$ (see for details [27]). After simple algebra we

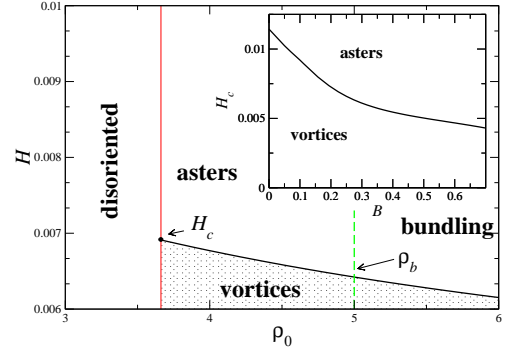


FIG. 6: Phase boundaries obtained from the linear stability analysis of the aster solution for $B^2 = 0.05$, dashed line shows bundling instability limit $\rho_0 = \rho_b = 5$. Inset: Position of cr

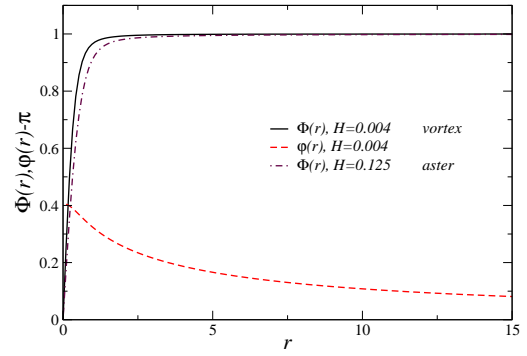


FIG. 7: Stationary vortex and aster solutions $\tau_x + i\tau_y = \Phi(r) \exp[i\theta + i\varphi(r)]$ to Eq. (63), for $\rho_0 = 4$, $B^2 = 0.05$.

obtain that for $r \rightarrow \infty$ the adjoint operator is of the form

$$\hat{L}^\dagger \equiv \bar{D}\partial_r^2 - a_2 H \partial_r \quad (67)$$

Substituting the solution to Eq. (67) in the form $w^\dagger \sim \exp[pr]$ we obtain that there are two solutions: $p = 0$ which describes the neutral translation mode, and the non-trivial solution

$$p = a_2 H / \bar{D} \quad (68)$$

Since due to interaction the well-separated asters produce only small perturbations to their shape, these perturbations can be treated in linear approximation, and the exponent (68) characterizes asymptotic screening of the interaction between the asters analogous to the interaction of spiral waves in the Ginzburg-Landau equation, see Ref. [27] for details of analysis. Thus we obtain that perturbations produced due to interaction of well-separated asters decay as $w \sim \exp[-r/L_0]$ with the screening length $L = 1/p$, or in original units $L_0 = \bar{D}/a_2 H \sqrt{\epsilon} = \bar{D}/a_2 H \sqrt{\rho/\rho_c - 1}$ (see for details [27]). Screening length L_0 diverges for $H \rightarrow 0$ and at the threshold $\rho_0 \rightarrow \rho_c$. Similar analysis can be performed for vortices.

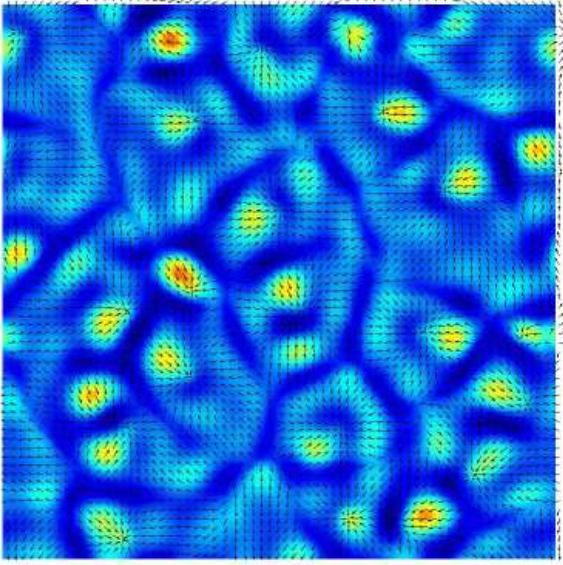


FIG. 8: Composite image of the density (colors) and orientation (arrows) fields in the regime of density instability. Density changes from $\rho_{max} \approx 10$ (red) to $\rho_{min} \approx 4$ (dark blue). Parameters: $B^2 = 0.05$, $\rho_0 = 6$, $H = 0.125$, domain of integration 80×80 units.

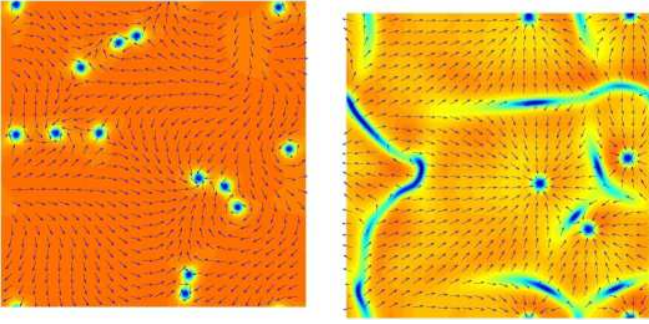


FIG. 9: Orientation τ for vortices ($H = 0.006$, left) and asters ($H = 0.125$, right) obtained from Eqs. (59),(60). Color code indicates the intensity of $|\tau|$ (red corresponds to maximum and blue to zero), $B^2 = 0.05$, $\rho_0 = 4$, domain of integration 80×80 units, time of integration 1000 units.

D. Numerical solution of full system

We also studied the full system (59),(60) numerically. Integration was performed in a two-dimensional square domain with periodic boundary conditions by the quasi-spectral method. For small H we observed vortices and for larger H asters, in agreement with the above analysis. Since vortices exist for smaller values of H , their screening length L is larger than for the asters because $L \sim 1/H$, see Eq. (68). Thus, the vortices interact stronger and are more keen to annihilate than asters. As seen in Fig. 9, asters have a unique orientation of the microtubules (here, towards the center). Asters with the opposite orientation of τ are unstable.

In large domains asters form a disordered network of cells with the cell size of the order of L_0 . Neighboring cells are separated by the “shock lines” terminated by saddle-type defects. The pattern of asters resembles a “frozen” glass state of spirals observed in the complex Ginzburg-Landau model [27, 28]. Starting from a random initial condition we observed initial merging and annihilation of asters. Eventually, annihilation slows down due to exponential weakening of the interaction of asters. For the same integration time the number of vortices is typically smaller than the number of aster due to the fact that the screening length of asters is smaller.

E. Drift instability of the asters

In experiments [4, 5] asters often are not stationary: they drift and coalesce. Surprisingly, in our numerical investigations of Eqs. (59), (60) we also observed that typically the center of an aster is unstable and develops a spontaneous acceleration instability, see Fig. 10. This instability is reminiscent of the instability of the core of spiral waves in the complex Ginzburg-Landau equation in a large dispersion limit, see Ref. [29]. This instability associated in Ref. [29] with the exponential growth of localized mode in the form $w_1(r) \exp[i\theta]$, which is similar to the translation mode and results in the displacement of the core. We have found that the instability can be suppressed by increasing the coefficients in front of the last term ($\sim \nabla^4 \rho$) in Eq. (59). In this context it is possible that the acceleration instability is just an artifact of the approximations made in the course of derivation, such as binary character of interactions of microtubules, small-gradient expansion, etc. Furthermore, for high density of the microtubules the prefactor in form of the cut-off term $\sim \nabla^4 \rho$ to should grow rapidly and dampen the instability. While at the moment there is no unambiguous experimental evidence of this instability (e.g. the drift of asters could be also attributed to gradients of microtubules or motor distributions, effects of the boundaries etc), we believe that this instability can be found in certain experimental conditions. To study the drift instability we prepared by the initial condition axisymmetric aster solution perturbed by the small amplitude noise. In the course of motion the solution breaks the axial symmetry, typical structure of the moving aster is shown in Figure 10. There is a small but noticeable (about 10%) increase of the density ρ and the amplitude of orientation $|\tau|$ behind the aster, for the immobile solution the position of the zero of τ and maximum of ρ coincides. The instability accelerates collisions and coalescence of asters. However the growth rate λ of the instability appears to be very small and aster solutions are well-preserved for a very long time (several hundreds of dimensionless units). Fig. 11 shows the velocity of aster core vs time for the parameters of Fig. 10. One clearly sees initial exponential growth of the aster velocity.

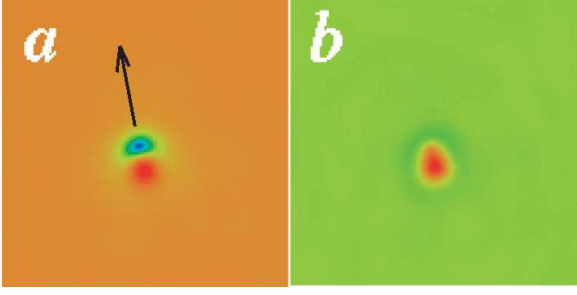


FIG. 10: Drift instability of asters for $H = 0.125, B = 0.06, \rho_0 = 4$, size of the image 40×40 at the moment of time $t = 300$. Left image shows $|\tau|$, right image shows ρ , arrow indicates the direction of drift. Color code: blue corresponds to zero, red corresponds to maximum.

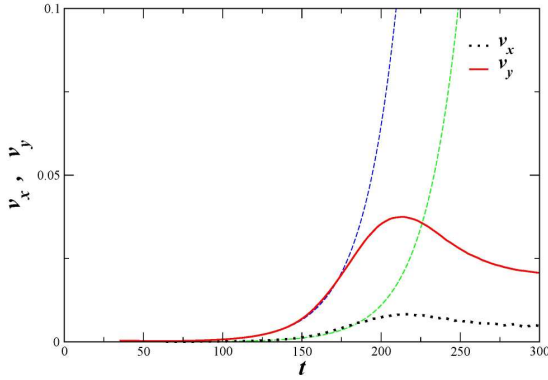


FIG. 11: Aster core velocity vs time for parameters of Fig. 10. Solid line shows v_y , dotted line shows v_x , dashed lines depict exponential fit $v \sim \exp(\lambda t)$ for first 150 units of time.

V. EFFECTS OF MOTORS ATTACHED TO THE BOTTOM PLATE

In the previous Sections we considered microtubules interacting with molecular motors freely floating in the solvent. However, in *in vitro* experiments it is difficult to prevent attachment of some fraction of motors to the bottom of the cell with one of their two heads. The other (free) head of the attached (absorbed) molecular motor then may bind to a microtubule and push it in the direction opposite its orientation. This effect was observed experimentally in Ref. [30] (referred to as microtubule gliding assays).

The effect of attached motors can be easily incorporated in the master equation

$$\frac{\partial P}{\partial t} = \frac{\partial^2 P}{\partial \phi^2} + \partial_i D_{ij} \partial_j P + \alpha \nabla \cdot (\mathbf{n} P) + Z_0 + Z_1(69)$$

Here α is the fraction of the attached motors, and the term $\mathbf{n} \nabla P$ account for the transport of the microtubules

in the direction opposite to their orientation vector $\mathbf{n} = [\cos \phi, \sin \phi]$. Terms $Z_{0,1}$ remain unchanged. It is easy to check that the drift term will generate additional linear terms $\alpha \pi \nabla \tau$ in Eq. (59) and $\alpha (4\pi)^{-1} \nabla \rho$ in Eq.(60).

It is useful to write Eq. (59) in the form of the mass conservation law

$$\rho_t = -\nabla \cdot \mathbf{J} \quad (70)$$

with the corresponding mass flux \mathbf{J} . The anisotropic part of the kernel generates mass flux which is second order in the gradients of ρ, τ . The the lowest-order term $\mathbf{J} \sim \tau$ in the expression for flux is generated by the motors attached to the substrate and is similar to that of self-propelled particles, see e.g. [26]. In the situation considered in Sec. IV A this term is prohibited by the momentum conservation: the molecular motors produce only internal forces which cannot displace the center of mass of the system. However this is not the case when some of the motors are attached to the substrate. In Ref. [14] similar contribution to the flux were attributed to the net displacement of the center of the microtubule pair due to the anisotropy of the viscous drag coefficient. However this pure hydrodynamic effect is probably smaller than the advection produced by the motors absorbed at the substrate.

While the fraction of absorbed motors α might be small, it still can produce a considerable effect because it generates the lowest-order transport term in Eqs. (59),(60). Numerical studies of Eqs. (59),(60) with additional α -terms reveal that the qualitative features are not very sensitive to the presence of these terms for small $\alpha \ll 1$, as long as the diffusive transport in the equation for the density ρ dominates advection. However, for moderate α we observed that the aster and vortices become even less localized, see Fig. 12. This delocalization is due to the fact that the absorbed motors advect the microtubules in the direction opposite their orientation. Consequently, these motors move the tubules *from the asters* and make a small depression of density for $\alpha \neq 0$ contrary to the density peak for $\alpha = 0$, compare images on Fig. 12. Similar results are also obtained for vortices. Remarkably, the suppression of density of microtubules in the core of vortex is observed experimentally, see Fig. 2a in Ref. [5].

The absorbed motors, resulting in the displacement of the center of mass of the microtubules system, may explain rotation of vortices absent in our previous analysis. Indeed, since these motors generate net motion of individual microtubules with the velocity $\sim \alpha$, they can support rotating configurations similar to that observed in the system of vibrated rods [26]. Obviously no rotation anticipated for asters due to pure radial orientation of microtubules: the forces induced by motors attached to substrate will be compensated by “pressure” gradient due to redistribution of density of microtubules. In contrary, the rotation is present for vortices. Far away from the core the distinction between vortex and aster disappears, the rotation is localized only at the core of

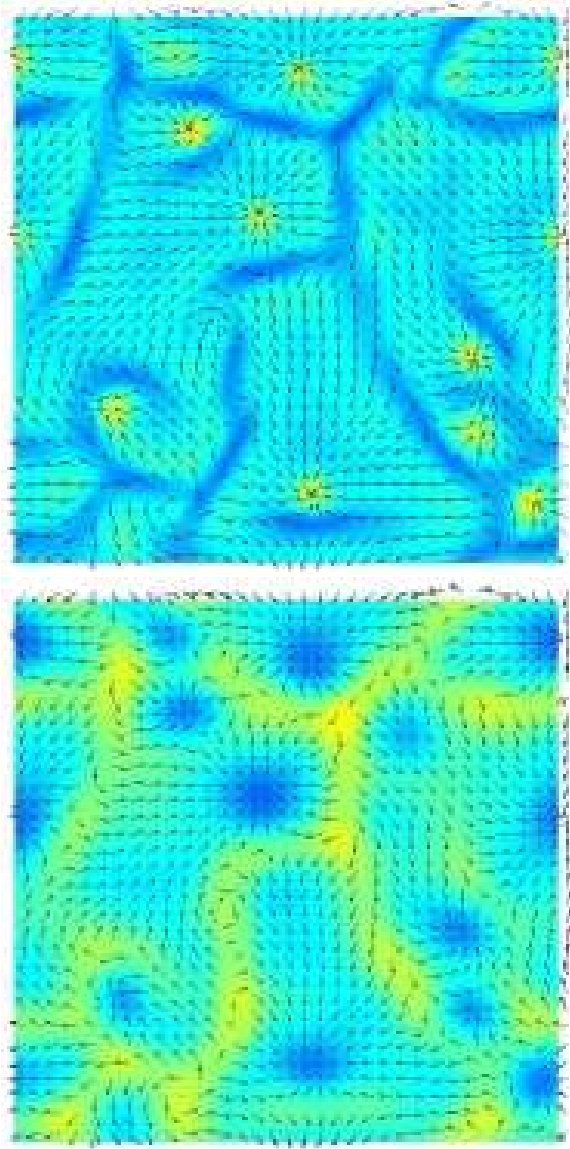


FIG. 12: Comparison between density distributions (colors) without (upper image) and with drift term ($\alpha = 0.004$). Arrows show corresponding orientation. overall change in the density about 5%, $B^2 = 0.05$, $\rho_0 = 4$, $H = 0.1$, domain of integration 80×80 .

the vortex where the phase ϕ is different from π . Since the amplitude of orientation vector τ grows almost linearly from the vortex core and reaches asymptotic value $\tau_0 \approx \sqrt{\epsilon/A_0}$ at the distance about $1 - 2$ dimensionless units (see Fig. 7), the rotation frequency of the vortex core $\omega \approx \alpha\tau_0$. Indeed, rotation of the vortex core was observed experimentally. For the parameters of our numerical studies the frequency ω is very small due to the smallness of $\alpha = 0.004$, thus during the time of numerical experiment (< 1000 dimensionless units of time) the vortex core turned only the fraction of full circle.

VI. INHOMOGENEOUS DISTRIBUTION OF MOTORS

In previous Sections we always assumed a homogeneous bulk distribution of molecular motors (however we took into account local inhomogeneity of bound motor concentration on the scale of a single tubule to account for the collision rate anisotropy in Sec.III B). This assumption was justified by the fact that the diffusion of motors is about two orders of magnitude larger than of microtubules. However experiments indicate that even despite this strong diffusion, molecular motors aggregate in the core regions of asters and vortices due to the directed transport of motors by microtubules [7].

To describe the dynamics of the motor concentration we again invoke the equations for free m_f and bound m_b motor concentrations, but unlike Sec. III B, we will coarse-grain these distributions on the scale much larger than the size of individual filament similar to Ref. [7] (see also [8, 9, 10]) The populations m_b, m_f obey the advection-diffusion equations [7] (compare with Sec. III B)

$$\begin{aligned}\partial_t m_f &= D\nabla^2 m_f - \rho(p^{on} m_f - p^{off} m_b) \\ \partial_t m_b &= -\zeta \nabla m_b \tau + \rho(p^{on} m_f - p^{off} m_b)\end{aligned}\quad (71)$$

where p^{on}, p^{off} are the rates of binding/unbinding of motor to the microtubules, D, ζ are diffusion/advection coefficients accordingly.

If we assume that the distributions of m_f, m_b are smooth and the binding/unbinding rates are large, then the r.h.s. Eqs. (71) is dominated by the last term describing binding/unbinding of the motors, leading to the local balance relation between m_f, m_b

$$p^{on} m_f \approx p^{off} m_b \quad (72)$$

Then we can reduce system (71) to a single equation for the total motor density $m = m_f + m_b$:

$$\partial_t m = D_0 \nabla^2 m - \zeta_0 \nabla m \tau \quad (73)$$

where $D_0 = D p^{off} / (p^{off} + p^{on})$ and $\zeta_0 = \zeta p^{on} / (p^{off} + p^{on})$.

Accordingly, we need to modify the expression for the interaction kernel Eq. (45) in order to include the effect of the motors. The simplest way to include inhomogeneous motor density into the kernel is the following,

$$W_m = m \left(\frac{\mathbf{r}_1 + \mathbf{r}_2}{2} \right) W(\mathbf{r}_1 - \mathbf{r}_2, \phi_1 - \phi_2) \quad (74)$$

where W is given by Eq. (45). Taking the motor concentration in the middle point $(\mathbf{r}_1 + \mathbf{r}_2)/2$ is necessary to preserve the mass conservation law. Repeating the calculations presented in the previous sections one can derive equations similar to Eqs. (59),(60) but with the motor density as an independent field. However the resulting equations are very cumbersome, especially for the transport term in Eq. (59).

One can simplify the problem considerably utilizing again the fact that the motor diffusion is high, and therefore, the distribution of m is smooth. Then, one can ne-

glect the derivatives of m where it is appropriate, and the resulting equations assume the form:

$$\begin{aligned} \partial_t \rho = & \nabla^2 \left[\frac{\rho}{32} - \frac{m B^2 \rho^2}{16} \right] + \alpha \pi \nabla \cdot \tau \\ & - \frac{\pi B^2 H}{16} [3 \nabla m (\tau \nabla^2 \rho - \rho \nabla^2 \tau) + 2 \partial_i m (\partial_j \rho \partial_j \tau_i - \partial_i \rho \partial_j \tau_j)] - \frac{7 \rho_0 m_0 B^4}{256} \nabla^4 \rho \end{aligned} \quad (75)$$

$$\begin{aligned} \partial_t \tau = & \frac{5}{192} \nabla^2 \tau + \frac{1}{96} \nabla (\nabla \cdot \tau) + \frac{\alpha}{4\pi} \nabla \rho + ((4/\pi - 1)m\rho - 1) \tau \\ & - A_0 |\tau|^2 \tau - H m \left[\frac{\nabla \rho^2}{16\pi} - \left(\pi - \frac{8}{3} \right) \tau (\nabla \cdot \tau) - \frac{8}{3} (\tau \nabla) \tau \right] + \frac{B^2 \rho_0 m_0}{4\pi} \nabla^2 \tau \end{aligned} \quad (76)$$

Thus, motor density is included in the lowest order in gradient expansion. We also included terms $\sim \alpha$ describing the transport of microtubules by the absorbed motors. Again for simplicity we replaced the motor density m by its mean value m_0 in the last terms in Eqs. (75),(76).

We carried out numerical studies of Eqs. (75),(76). The values of the parameters D_0, ξ_0 can be estimated from the experimental conditions, in our dimensionless units $D_0 \sim 1..5$ and $\xi_0 \sim 1$.

Selected results are shown in Fig. 13,14. In agreement with experiment, we observed that motors tend to accumulate in the center of an aster or a vortex, see Fig.13,14. Otherwise, qualitative behavior of formation of asters and vortices remains the same. As seen in Figure 14, initial multi-aster state coarsens and leads to the formation of a network of large asters separated by the domain walls.

VII. CONCLUSIONS

In this paper we derived continuous equations for the evolution of microtubule concentration and orientation due to their interaction via molecular motors. We found that an initially disordered system exhibits an ordering instability qualitatively similar to the nematic phase transition in ordinary polymers at high density. The important difference is that here the ordering instability is mediated by molecular motors and can occur at arbitrary low densities of microtubules. At the nonlinear stage, the instability leads to the experimentally observed formation of asters and vortices. Similar vortices were observed in a system of interacting granular rods [26, 31]. While we find that it suffices to consider only the density of tubules to explain the basic phenomenology, a better agreement with experiment is obtained when we include variable motor density and the motors attachment to the substrate [7, 8, 9].

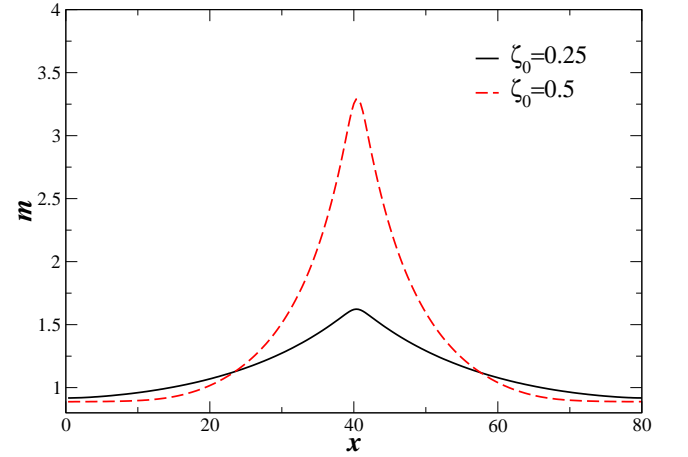


FIG. 13: Motor concentration profiles m for different values of ζ_0 for isolated aster for $H = 0.125, B = 0.06, D = 5$, and $m_0 = 1, \rho_0 = 4$.

Many aspects of self-assembly in tubule-motor systems require further investigation. In particular, we anticipate that flexibility of the microtubules may have a strong effect on the details of interaction, the question which we plan to address in future work. Another interesting question is role of the hydrodynamic interaction between the microtubules and effects of fluctuations on the orientation transition. Furthermore, our theory is derived in the limit of small density of the microtubules and takes into account only binary interactions among tubules. Certainly, multiparticle interactions are important in the high density state, such as bundles. Generalization of our work to the multiparticle interaction is a very challenging problem.

There are many predictions following from our analy-

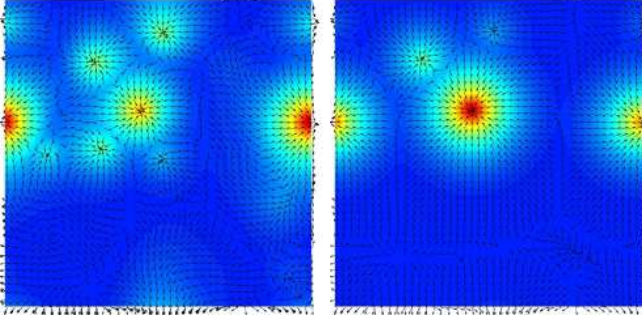


FIG. 14: Color-coded images of density of motors at $t = 200$ (left) and $t = 1000$ (right), red corresponds to maximum density and blue to minimum density, domain size is 80×80 units, $\zeta_0 = 0.5$, $H = 0.125$, $D = 5$, $m_0 = 1$. Arrows show orientation of microtubules.

sis which possibly deserve experimental verification. For

example, we find that the anisotropy of the interaction kernel is associated with the inhomogeneous density of motors along the microtubules. We observed that the motors attached to the substrate reduce the density of microtubules in the cores of asters and vortices. We predicted an acceleration instability which leads to a drift of isolated asters. Hopefully, new generations of experiments will be able to address these issues.

We thank Jacques Prost, Anthony Maggs, Leo Kadanoff and Valerii Vinokur for useful discussions. This work was supported by the U.S. Department of Energy, grants W-31-109-ENG-38 (IA) and DE-FG02-04ER46135 (LT).

APPENDIX A: CONTINUUM EQUATIONS FOR ARBITRARY γ, ϕ_0

We assume that two rods interact when angle between them is less or equal ϕ_0 independent of their spatial location. The master equation reads

$$\begin{aligned} \frac{\partial P(\phi, t)}{\partial t} = D_r \frac{\partial^2 P(\phi, t)}{\partial \phi^2} \\ + g \int_0^{\phi_0/2} \int_0^{2\pi} 2dydx P(x+y, t) P(x-y, t) [\delta(\phi - \gamma(x-y) - (1-\gamma)(x+y)) - \delta(\phi - x - y)] \\ + g \int_{\pi-\phi_0/2}^{\pi} \int_0^{2\pi} 2dydx P(x+y, t) P(x-y, t) [\delta(\phi - \gamma(x-y) - (1-\gamma)(x+y+2\pi)) - \delta(\phi - x - y)] \end{aligned} \quad (A1)$$

where $x = (\phi_1 + \phi_2)/2, y = (\phi_2 - \phi_1)/2$ (take into account that $d\phi_1 d\phi_2 = 2dxdy$), and g is the collision rate, and we also included thermal diffusion of rods orientation $\propto D_r$.

Performing integration over x from 0 to 2π , we get

$$\begin{aligned} \frac{\partial P(\phi, t)}{\partial t} = D_r \frac{\partial^2 P(\phi, t)}{\partial \phi^2} + 2g \int_0^{\phi_0/2} dy [P(\phi + 2\gamma y, t) P(\phi + 2(\gamma - 1)y, t) - P(\phi, t) P(\phi - 2y, t)] \\ + 2g \int_{\pi-\phi_0/2}^{\pi} dy [P(\phi + 2\gamma y + 2\pi\gamma, t) P(\phi + 2(\gamma - 1)y + 2\pi\gamma, t) - P(\phi, t) P(\phi - 2y, t)] \end{aligned} \quad (A2)$$

Changing variable $y \rightarrow y + \pi$ in the second term in (A2), we obtain

$$\frac{\partial P(\phi, t)}{\partial t} = D_r \frac{\partial^2 P(\phi, t)}{\partial \phi^2} + 2g \int_{-\phi_0/2}^{\phi_0/2} dy [P(\phi + 2y\gamma, t) P(\phi + 2y(\gamma - 1), t) - P(\phi, t) P(\phi - 2y, t)] \quad (A3)$$

The case when all rods interact corresponds to $\phi_0 = \pi$, and Eq.(A3) simplifies to

$$\frac{\partial P(\phi, t)}{\partial t} + gP(\phi, t) = D_r \frac{\partial^2 P(\phi, t)}{\partial \phi^2} + 2g \int_{-\pi/2}^{\pi/2} dy [P(\phi + 2y\gamma, t) P(\phi + 2y(\gamma - 1), t) - P(\phi, t) P(\phi - 2y, t)] \quad (A4)$$

By substitution $y \rightarrow w/2$ Eq. (A3) can be transformed into the form

$$\frac{\partial P(\phi, t)}{\partial t} - \frac{\partial^2 P(\phi, t)}{\partial \phi^2} = \int_{-\phi_0}^{\phi_0} dw [P(\phi + w\gamma, t) P(\phi + w(\gamma - 1), t) - P(\phi, t) P(\phi - w, t)] \quad (A5)$$

where we changed variables $t \rightarrow D_r t, P \rightarrow gP/D_r$.

Let us consider a Fourier expansion of the probability distribution

$$P(\phi, t) = \sum_{k=-\infty}^{\infty} P_k(t) e^{ik\phi} \quad (\text{A6})$$

where $P_{-k} = P_k^*$. The Fourier harmonics P_k are given by angular averages of $\exp(ik\phi)$, see Eq. (6). The constant zeroth harmonic $P_0 = 1/2\pi\rho$, where ρ is the number density,

$$\rho = \int_0^{2\pi} d\phi P(\phi, \mathbf{r}) = 2\pi P_0 \quad (\text{A7})$$

and the real and imaginary parts of P_1 represent the components of the orientation vector $\tau = (\langle \cos \phi \rangle, \langle \sin \phi \rangle)$. Accordingly, $\tau_x + i\tau_y = \langle \exp[i\phi] \rangle = P_1^*$.

After substitution of (A6) into Eq.(A5) we obtain the infinite series of equations for P_k

$$\dot{P}_k + k^2 P_k = 2\phi_0 \sum_n \sum_m P_n P_m (S[\phi_0(n\gamma + m(\gamma - 1))] - S(m\phi_0)) \delta_{n+m,k} \quad (\text{A8})$$

where $S(x) = \sin x/x$, and $\delta_{n+m,k}$ is the Kroneker symbol.

For $\phi_0 = \pi$, the latter equation simplifies to

$$\dot{P}_k + (k^2 + 1)P_k = 2\pi \sum_n \sum_m P_n P_m S[\pi(n\gamma + m(\gamma - 1))] \delta_{n+m,k} \quad (\text{A9})$$

Now we have to truncate this series. Assuming $P_n = 0$ for all $|n| > 2$, from Eq.(A8) one obtains $\dot{P}_0 = 0$,

$$\begin{aligned} \dot{P}_1 + P_1 &= P_0 P_1 2\phi_0 [S[\phi_0(\gamma - 1)] + S[\phi_0\gamma] - S(\phi_0) - 1] \\ &+ 2\phi_0 P_2 P_1^* [S[\phi_0(\gamma + 1)] + S[\phi_0(\gamma - 2)] - S(2\phi_0) - S(\phi_0)] \end{aligned} \quad (\text{A10})$$

and

$$\dot{P}_2 + 4P_2 = P_0 P_2 2\phi_0 [S[2\phi_0(\gamma - 1)] + S[2\phi_0\gamma] - S(2\phi_0) - 1] + 2\phi_0 P_1^2 [S[\phi_0(2\gamma - 1)] - S(\phi_0)] \quad (\text{A11})$$

Neglecting the time derivative \dot{P}_2 , we obtain $P_2 = AP_1^2$ with

$$A = \frac{S[\phi_0(2\gamma - 1)] - S(\phi_0)}{2/\phi_0 - (S[2\phi_0(\gamma - 1)] + S[2\phi_0\gamma] - S(2\phi_0) - 1)\rho/2\pi} \quad (\text{A12})$$

That allows us to close the equation for P_1 ,

$$\begin{aligned} \dot{P}_1 + P_1 &= \rho P_1 \phi_0 \pi^{-1} [S[\phi_0(\gamma - 1)] + S[\phi_0\gamma] - S(\phi_0) - 1] \\ &+ 2A\phi_0 |P_1|^2 P_1 [S[\phi_0(\gamma + 1)] + S[\phi_0(\gamma - 2)] - S(2\phi_0) - S(\phi_0)] \end{aligned} \quad (\text{A13})$$

For $\phi_0 = \pi$,

$$\dot{P}_1 + (1 + \rho)P_1 = \rho P_1 [S[\pi(\gamma - 1)] + S[\pi\gamma]] + 2\pi A_0 |P_1|^2 P_1 [S[\pi(\gamma + 1)] + S[\pi(\gamma - 2)]] \quad (\text{A14})$$

where

$$A_0 = \frac{2\pi S[\pi(2\gamma - 1)]}{4 - (S[2\pi(\gamma - 1)] + S[2\pi\gamma] - 1)\rho} \quad (\text{A15})$$

As seen from this equation, for $0 < \gamma < 1$ we obtain an ordering instability which for large enough $\rho > \rho_c$ leads to a spontaneous alignment of filaments.

APPENDIX B: EVALUATION OF TERMS Z_0, Z_1

1. Isotropic term Z_0 .

We introduce new variable $\xi = \mathbf{r} - \mathbf{r}_1$, and obtain after simple algebra

$$Z_0 = \int d\xi \int_{-\phi_0}^{\phi_0} dw W_0(|\xi|) [P(\mathbf{r} - \xi/2, \phi + w\gamma, t)P(\mathbf{r} + \xi/2, \phi + w(\gamma - 1), t) - P(\mathbf{r}, \phi, t)P(\mathbf{r} - \xi, \phi - w, t)] \quad (\text{B1})$$

Now we assume that the probability distributions are smooth functions of spatial coordinates on the scale of the rod length l , and expand them near \mathbf{r} ,

$$P(\mathbf{r} + \xi, \phi, t) = P(\mathbf{r}, \phi, t) + (\xi \cdot \nabla)P(\mathbf{r}, \phi, t) + \frac{1}{2}(\xi \cdot \nabla)^2 P(\mathbf{r}, \phi, t) + O(\xi^3), \quad (\text{B2})$$

Performing integration over ξ using kernel (45), we get

$$\begin{aligned} Z_0 &= \int_{-\phi_0}^{\phi_0} dw [P(\mathbf{r}, \phi + w\gamma, t)P(\mathbf{r}, \phi + w(\gamma - 1), t) - P(\mathbf{r}, \phi, t)P(\mathbf{r}, \phi - w, t)] \\ &+ \frac{b^2}{16} \int_{-\phi_0}^{\phi_0} dw [-2\nabla P(\mathbf{r}, \phi + w\gamma, t)\nabla P(\mathbf{r}, \phi + w(\gamma - 1), t) \\ &+ \nabla^2 P(\mathbf{r}, \phi + w\gamma, t)P(\mathbf{r}, \phi + w(\gamma - 1), t) + P(\mathbf{r}, \phi + w\gamma, t)\nabla^2 P(\mathbf{r}, \phi + w(\gamma - 1), t) - 4P(\mathbf{r}, \phi, t)\nabla^2 P(\mathbf{r}, \phi - w, t)] \end{aligned} \quad (\text{B3})$$

Now we expand P 's in the Fourier series over ϕ , $P(\mathbf{r}, \phi, t) = \sum_n P_n e^{in\phi}$. The k th Fourier component of Z_0 reads

$$\begin{aligned} Z_0^k &= 2\phi_0 \sum_n \sum_m \delta_{n+m,k} P_n P_m [S[\phi_0(n\gamma + m(\gamma - 1))] - S(m\phi_0)] \\ &+ \frac{b^2\phi_0}{8} \sum_n \sum_m \delta_{n+m,k} [(-2\nabla P_n \nabla P_m + \nabla^2 P_n P_m + P_n \nabla^2 P_m)S[n\gamma\phi_0 + m(\gamma - 1)\phi_0] - 4P_n \nabla^2 P_m S(m\phi_0)] \end{aligned} \quad (\text{B4})$$

The first sum in Eq.(B4) coincides with the spatially uniform case (A8). For $k = 0$ we obtain (keeping only terms up to $|n|, |m| = 1$)

$$Z_0^0 = -\frac{b^2\phi_0}{8} [\nabla^2(P_0^2) + 2\nabla^2(|P_1|^2)S(\phi_0)] \quad (\text{B5})$$

For $k = 1$

$$\begin{aligned} Z_0^1 &= 2\phi_0 P_0 P_1 [S[\phi_0(\gamma - 1)] + S[\phi_0\gamma] - S(\phi_0) - 1] + 2\phi_0 P_2 P_1^* [S[\phi_0(\gamma + 1)] + S[\phi_0(\gamma - 2)] - S(2\phi_0) - S(\phi_0)] \\ &+ \frac{b^2\phi_0}{8} [(\nabla^2 P_0 P_1 + P_0 \nabla^2 P_1 - 2\nabla P_0 \nabla P_1)(S[\gamma\phi_0] + S[(\gamma - 1)\phi_0]) - 4P_0 \nabla^2 P_1 S[\phi_0] - 4P_1 \nabla^2 P_0] \\ &+ \frac{b^2\phi_0}{8} [(-2\nabla P_1^* \nabla P_2 + \nabla^2 P_1^* P_2 + P_1^* \nabla^2 P_2)S[(2 - \gamma)\phi_0] + (-2\nabla P_2 \nabla P_1^* + \nabla^2 P_2 P_1^* + P_2 \nabla^2 P_1^*)S[(1 + \gamma)\phi_0] \\ &- 4P_1^* \nabla^2 P_2 S(2\phi_0) - 4P_2 \nabla^2 P_1^* S(\phi_0)] \end{aligned} \quad (\text{B6})$$

[this equations derived with the aid of Mathematica [32]].

We can again use the expression $P_2 = AP_1^2$ with constant A obtained for the spatially uniform case (A12).

Now, if we set $\phi_0 = \pi$, $\gamma = 1/2$ and neglect higher order terms in the differential operators, we obtain

$$\begin{aligned} Z_0^0 &= -\frac{b^2\pi}{8} \nabla^2(P_0^2) \\ Z_0^1 &= 2P_0 P_1 (4 - \pi) - \frac{8}{3} P_2 P_1^* + \frac{b^2}{2} [\nabla^2(P_0 P_1) - 4\nabla P_0 \nabla P_1 - \pi P_1 \nabla^2 P_0 - (\nabla^2(P_2 P_1^*) - 4\nabla P_1^* \nabla P_2)/3] \end{aligned}$$

2. Anisotropic term Z_1 .

For compactness of notations we introduce the following definitions $z = x + iy, \psi = n_x + in_y = \exp[i\phi]$. Scalar product assumes the form $\mathbf{r} \cdot \mathbf{n} = \text{Re}(z^* \exp[i\phi])$. Now Eq. (58) can be written in the form

$$Z_1 = \int d\mathbf{r}_1 \int_{-\phi_0}^{\phi_0} dw \left[2W_0(2(\mathbf{r}_1 - \mathbf{r})) \text{Re}(2(z_1 - z)^*(e^{i(\phi+\gamma w)} - e^{i(\phi+(\gamma-1)w)})) P(\mathbf{r}_1, \phi + \gamma w, t) P(2\mathbf{r} - \mathbf{r}_1, \phi + (\gamma - 1)w, t) \right. \\ \left. - W_0(\mathbf{r}_1 - \mathbf{r}) \text{Re}((z_1 - z)^*(e^{i(\phi-w)} - e^{i\phi})) P(\mathbf{r}, \phi, t) P(\mathbf{r}_1, \phi - w, t) \right] \quad (\text{B7})$$

Let us introduce $\boldsymbol{\xi} = 2(\mathbf{r}_1 - \mathbf{r})$, $\zeta = 2(z_1 - z)$ in the first integrand of Eq.(B7) and $\boldsymbol{\xi} = \mathbf{r}_1 - \mathbf{r}$, $\zeta = z_1 - z$ in the second, and obtain

$$Z_1 = \int d\boldsymbol{\xi} \int_{-\phi_0}^{\phi_0} dw W_0(|\boldsymbol{\xi}|) \left[\text{Re}(\zeta^*(e^{i(\phi+\gamma w)} - e^{i(\phi+(\gamma-1)w)})) P(\mathbf{r} + \boldsymbol{\xi}/2, \phi + \gamma w, t) P(\mathbf{r} - \boldsymbol{\xi}/2, \phi + (\gamma - 1)w, t) \right. \\ \left. - \text{Re}(\zeta^*(e^{i(\phi-w)} - e^{i\phi})) P(\mathbf{r}, \phi, t) P(\mathbf{r} + \boldsymbol{\xi}, \phi - w, t) \right] \quad (\text{B8})$$

Now we again make use of the Fourier expansion $P(\mathbf{r}, \phi, t) = \sum_n P_n(\mathbf{r}, t) e^{in\phi}$. Multiplying Eq.(B8) by $(2\pi)^{-1} e^{-ik\phi}$ and integrating over ϕ from 0 to 2π , we get

$$Z_1^k = \frac{1}{2\pi} \int d\boldsymbol{\xi} \int_0^{2\pi} d\phi \int_{-\phi_0}^{\phi_0} dw W_0(|\boldsymbol{\xi}|) e^{-ik\phi} \left[\text{Re}(\zeta^*(e^{i(\phi+\gamma w)} - e^{i(\phi+(\gamma-1)w)})) P(\mathbf{r} + \boldsymbol{\xi}/2, \phi + \gamma w, t) P(\mathbf{r} - \boldsymbol{\xi}/2, \phi + (\gamma - 1)w, t) \right. \\ \left. - \text{Re}(\zeta^*(e^{i(\phi-w)} - e^{i\phi})) P(\mathbf{r}, \phi, t) P(\mathbf{r} + \boldsymbol{\xi}, \phi - w, t) \right] \quad (\text{B9})$$

Using periodicity in ϕ we shift variables $\phi \rightarrow \phi - \gamma w$ in the first integrand:

$$Z_1^k = \frac{1}{2\pi} \int d\boldsymbol{\xi} \int_0^{2\pi} d\phi \int_{-\phi_0}^{\phi_0} dw W_0(|\boldsymbol{\xi}|) e^{-ik\phi} \text{Re}(\zeta^*(e^{i\phi} - e^{i(\phi-w)})) \\ [P(\mathbf{r} + \boldsymbol{\xi}/2, \phi, t) P(\mathbf{r} - \boldsymbol{\xi}/2, \phi - w, t) e^{ik\gamma w} + P(\mathbf{r}, \phi, t) P(\mathbf{r} + \boldsymbol{\xi}, \phi - w, t)] \quad (\text{B10})$$

Changing variables $\phi \rightarrow \phi + w$ and then $w \rightarrow -w$ where appropriate, we obtain

$$Z_1^k = \frac{1}{2\pi} \int d\boldsymbol{\xi} \int_0^{2\pi} d\phi \int_{-\phi_0}^{\phi_0} dw W_0(|\boldsymbol{\xi}|) e^{-ik\phi} \text{Re}(\zeta^* e^{i\phi}) \\ [P(\mathbf{r} + \boldsymbol{\xi}/2, \phi, t) P(\mathbf{r} - \boldsymbol{\xi}/2, \phi - w, t) e^{ik\gamma w} - P(\mathbf{r} + \boldsymbol{\xi}/2, \phi - w, t) P(\mathbf{r} - \boldsymbol{\xi}/2, \phi, t)] e^{ik(1-\gamma)w} \\ + P(\mathbf{r}, \phi, t) P(\mathbf{r} + \boldsymbol{\xi}, \phi - w, t) - P(\mathbf{r}, \phi - w, t) P(\mathbf{r} + \boldsymbol{\xi}, \phi, t) e^{ikw} \quad (\text{B11})$$

Let us consider again the zeroth and first moments only. For Z_1^0 we get

$$Z_1^0 = \frac{1}{2\pi} \int d\boldsymbol{\xi} \int_0^{2\pi} d\phi \int_{-\phi_0}^{\phi_0} dw W_0(|\boldsymbol{\xi}|) \text{Re}(\zeta^* e^{i\phi}) \\ [P(\mathbf{r} + \boldsymbol{\xi}/2, \phi, t) P(\mathbf{r} - \boldsymbol{\xi}/2, \phi - w, t) - P(\mathbf{r} + \boldsymbol{\xi}/2, \phi - w, t) P(\mathbf{r} - \boldsymbol{\xi}/2, \phi, t)] \\ + P(\mathbf{r}, \phi, t) P(\mathbf{r} + \boldsymbol{\xi}, \phi - w, t) - P(\mathbf{r}, \phi - w, t) P(\mathbf{r} + \boldsymbol{\xi}, \phi, t) \quad (\text{B12})$$

After cumbersome transformations in Mathematica it can be reduced to

$$Z_1^0 = \frac{1}{64\pi} \int_0^{2\pi} d\phi \int_{-\phi_0}^{\phi_0} dw [3 \text{Re}(\bar{\nabla}^* \exp(i\phi)) (P(\phi) \Delta P(\phi - w) - P(\phi - w) \Delta P(\phi)) \\ - 2 \text{Im}(\bar{\nabla}^* \exp(i\phi)) (P(\phi)_y P(\phi - w)_x - P(\phi)_x P(\phi - w)_y)] \quad (\text{B13})$$

(here $\bar{\nabla} = \partial_x + i\partial_y$, $\bar{\nabla}^* = \partial_x - i\partial_y$). Performing integration over ϕ and w , we obtain

$$Z_1^0 = \frac{\pi}{32} \left[3\bar{\nabla}^* (P_{-1}\Delta P_0 - P_0\Delta P_{-1}) - \frac{2}{i} (\bar{\nabla}^* (\partial_y P_{-1}\partial_x P_0 - \partial_x P_{-1}\partial_y P_0)) \right] + c.c. \quad (B14)$$

This expression can be written in the vector form

$$Z_1^0 = \frac{\pi}{16} \left[3\bar{\nabla} \cdot (\tau\Delta\rho - \rho\Delta\tau) - 2\frac{\partial}{\partial x} (\partial_y\tau_y\partial_x\rho - \partial_x\tau_y\partial_y\rho) + 2\frac{\partial}{\partial y} (\partial_y\tau_x\partial_x\rho - \partial_x\tau_x\partial_y\rho) \right]$$

Similarly, after some algebra we also obtain the anisotropic part of the first moment, which for $\gamma = 1/2$ reads

$$Z_1^1 = \frac{b^2}{4\pi} \int_0^{2\pi} d\phi \int_{-\phi_0}^{\phi_0} dw e^{-i\phi} \left[\text{Re}(e^{i\phi}\bar{\nabla}^*)P(\mathbf{r}, \phi, t)P(\mathbf{r}, \phi - w, t) - P(\mathbf{r}, \phi, t)\text{Re}(e^{i\phi}\bar{\nabla}^*)P(\mathbf{r}, \phi - w, t) \right] e^{iw/2} \\ + P(\mathbf{r}, \phi, t)\text{Re}(e^{i\phi}\bar{\nabla}^*)P(\mathbf{r}, \phi - w, t) - P(\mathbf{r}, \phi - w, t)\text{Re}(e^{i\phi}\bar{\nabla}^*)P(\mathbf{r}, \phi, t) e^{iw} \quad (B15)$$

Eq. (B15) can be written as

$$Z_1^1 = \frac{b^2}{4\pi} \int_0^{2\pi} d\phi \int_{-\phi_0}^{\phi_0} dw e^{-i\phi} (1 - e^{iw/2}) \\ \left[e^{iw/2} \text{Re}(e^{i\phi}\bar{\nabla}^*)P(\mathbf{r}, \phi, t)P(\mathbf{r}, \phi - w, t) + P(\mathbf{r}, \phi, t)\text{Re}(e^{i\phi}\bar{\nabla}^*)P(\mathbf{r}, \phi - w, t) \right] \quad (B16)$$

Now performing integration over ϕ, w we obtain

$$Z_1^1 = \frac{\phi_0 b^2}{2} \sum_{m=0}^{\infty} \left[(S((1/2 - m)\phi_0) - S((1 - m)\phi_0)) (\bar{\nabla}^* P_{-m} P_m + \bar{\nabla} P_{2-m} P_m) \right. \\ \left. + (S(m\phi_0) - S((1/2 - m)\phi_0)) (\bar{\nabla}^* P_m P_{-m} + \bar{\nabla} P_m P_{2-m}) \right] \quad (B17)$$

Substituting $\phi_0 = \pi$, and keeping only the first two moments, we obtain

$$Z_1^1 = \frac{\pi b^2}{2} \left[\bar{\nabla}^* P_0 P_0 - P_1 (\bar{\nabla}^* P_{-1} + \bar{\nabla} P_1) + S_{1/2} (\bar{\nabla}^* P_{-1} P_1 - \bar{\nabla}^* P_1 P_{-1}) + S_{3/2} (\bar{\nabla}^* P_1 P_{-1} - \bar{\nabla}^* P_{-1} P_1) \right] \quad (B18)$$

where $S_{1/2} = S(\pi/2)$ and $S_{3/2} = S(3\pi/2)$.

After some transformations we obtain

$$Z_1^1 = \frac{\pi b^2}{2} \left[\bar{\nabla}^* P_0 P_0 - (1 - S_{1/2} + S_{3/2}) (\bar{\nabla}^* P_{-1} P_1 + \bar{\nabla} P_1 P_1) - (S_{1/2} - S_{3/2}) (\bar{\nabla} P_1 P_1 + \bar{\nabla}^* P_1 P_{-1}) \right] \quad (B19)$$

In the vector form it gives

$$Z_1^1 = \frac{\pi b^2}{2} \left[\frac{1}{4\pi^2} \rho \nabla \rho - 2(1 - S_{1/2} + S_{3/2}) \tau \nabla \cdot \tau - 2(S_{1/2} - S_{3/2}) (\tau \nabla) \tau \right] \quad (B20)$$

Since $S_{1/2} = 2/\pi$, $S_{3/2} = -2/3\pi$, we obtain

$$Z_1^1 = b^2 \left[\frac{1}{8\pi} \rho \nabla \rho - \left(\pi - \frac{8}{3} \right) \tau (\nabla \cdot \tau) - \frac{8}{3} (\tau \nabla) \tau \right] \quad (B21)$$

-
- [1] J.Howard, *Mechanics of Motor Proteins and the Cytoskeleton*, Springer, New York, 2000.
[2] K.Takiguchi, J.Biochem. (Tokyo) **109**, 250 (1991)
[3] R. Urrutia, M.A. McNiven, J.P. Albanesi, D.B. Murphy,

- B. Kachar, Proc. Natl. Acad. Sci. USA **88**, 6701 (1991).
[4] F.J. Nédélec, T. Surrey, A. C. Maggs, and S. Leibler, Nature (London) **389**, 305 (1997).
[5] T. Surrey, F. Nédélec, S. Leibler, and E. Karsenti, Sci-

- ence, **292**, 1167 (2001).
- [6] D. Humphrey, C. Duggan, D. Saha, D. Smith, and J. Käs, *Nature* (London) **416**, 413 (2002).
 - [7] F. Nédélec, T. Surrey, A.C. Maggs, *Phys. Rev. Lett.* **86**, 3192 (2001)
 - [8] H.Y.Lee and M.Kardar, *Phys. Rev. E* **64**, 056113 (2001).
 - [9] J.Kim, Y. Park; B. Kahng, and H. Y. Lee, *J. Korean Phys. Soc.*, **42** 162 (2003).
 - [10] S. Sankararaman, G. I. Menon, and P. B. Sunil Kumar, *Phys. Rev. E* **70**, 031905 (2004)
 - [11] K. Kruse, J. F. Joanny, F. Jülicher, J. Prost, and K. Sekimoto, *Phys. Rev. Lett.* **92**, 078101 (2004)
 - [12] T.B. Liverpool and M.C.Marchetti, *Phys. Rev. Lett.* **90**, 138102 (2003)
 - [13] This point was challenged in F. Ziebert and W. Zimmermann, *Phys. Rev. Lett.* **93**, 159801 (2004)
 - [14] T.B.Liverpool and M.C.Marchetti, *Europhys. Lett.* **69**, 846 (2005)
 - [15] I.S. Aranson and L.S. Tsimring, *Phys. Rev. E* **71**, 050901(R) (2005)
 - [16] In the recent publication A. Ahmadi, T. B. Liverpool, and M. C. Marchetti [*Phys. Rev. E* **72**, 060901(R) (2005)] modified the phenomenological expression for the rotational flux first introduced in Ref. [12] and recovered the orientational instability first described in Ref. [15].
 - [17] E. Ben-Naim and P.L. Krapivsky, *Phys. Rev. E* **61**, R5 (2000).
 - [18] In the three-dimensional case, the drag coefficients ξ_{\parallel} , ξ_{\perp} for rod-like objects are different by the factor of two [24]. However, the relative difference between ξ_{\parallel} and ξ_{\perp} decreases in thin fluid films and membranes [25].
 - [19] R. B. Case, D. W. Pierce, N. Hom-Booher, C. L. Hart, and R. D. Vale, *Cell* **90**, 959 (1997)
 - [20] E. L. Grossman, Tong Zhou, and E. Ben-Naim *Phys. Rev. E* **55**, 4200 (1997)
 - [21] P.K. Haff, *J. Fluid. Mech.* **134**, 401 (1983)
 - [22] J.T. Jenkins and M.W. Richman, *Phys. Fluids*, **28**, 3485 (1985)
 - [23] Accumulation of motors at the polar end of microtubule was indeed observed experimentally in Ref. [19].
 - [24] M. Doi and S.F. Edwards, *The Theory of Polymer Dynamics*, Clarendon Press, Oxford, 1988.
 - [25] A. J. Levine, T. B. Liverpool, and F. C. MacKintosh *Phys. Rev. E* **69**, 021503 (2004)
 - [26] I.S.Aranson and L.S. Tsimring, *Phys. Rev. E* **67**, 021305 (2003).
 - [27] I.S.Aranson and L.Kramer, *Rev. Mod. Phys.* **74**, 99 (2002)
 - [28] C. Brito, I.S. Aranson and H. Chaté, *Phys. Rev. Lett.* **90**, 068301 (2003)
 - [29] I. Aranson, L. Kramer and A. Weber, *Phys. Rev. Lett.* **72**, 2316 (1994)
 - [30] Y.Vugmeyster, E.Berliner, J.Gelles, *Biochemistry* **37**, 747 (1998); R.D.Vale, R.A.Milligan, *Science* **288**, 88 (2000)
 - [31] D. L. Blair, T. Neicu, and A. Kudrolli, *Phys. Rev. E* **67**, 031303 (2003)
 - [32] Wolfram Research Inc.